Numerical simulations that characterize the effects of surfactant on droplets in shear flow

Mary Ann Drumright-Clarke

Dissertation submitted to the Faculty of the
Virginia Polytechnic Institute and State University
in partial fulfillment of the requirements for the degree of

Doctor of Philosophy
in
Mathematics

Yuriko Y. Renardy, Chair
Jong U. Kim
Tao Lin
Michael Renardy
ShuMing Sun
Robert C. Rogers

Date: April 15, 2002
Blacksburg, Virginia

Keywords: Volume of Fluid, VOF, Surfactant, Surfer++,
Reynolds Number, Capillary Number, Reduction,
Interface Tracking Methods

Numerical simulations that characterize the effects of surfactant on droplets in shear flow

Mary Ann Drumright-Clarke

(ABSTRACT)

Numerical simulations utilizing the code SURFER++ with the incorporation of an insoluble surfactant in the VOF scheme were conducted to characterize the effects of surfactant on a drop in shear flow. The drop is suspended in a matrix liquid. A parameter called reduction, which specifically relates to a percentage decrease in effective surface tension, is used to measure the surfactant amount on the interface. In a model system where reduction = 0.1, viscosity ratio = 1 and density ratio = 1, it was found that stable drops tend to be more elongated and less inclined to the primary flow direction than drops unexposed to surfactant. This can be explained by the location of surfactant at the interface as the drop evolves. Breaking drops also show a flattened angle, but exhibit shorter necks and faster time to break than similar drops without surfactant. As reduction increases, various physical characteristics of the drops change across Reynolds number.

To Granny Annie,
(I wish you could see this.)

Acknowledgments

So many people have helped me bring this dissertation to a reality. Foremost, I would like to recognize my advisor and friend, Yuriko Renardy. She has tolerated medical and family emergencies, my teaching load, my course load and my unusual personality for several years. She has been a faithful and wise mentor for me and I appreciate her very much.

Neither can I forget the many teachers who have encouraged me to stick with mathematics, despite my misgivings, throughout my graduate work. Dr. Marty Day, who tried to personally torture me with real analysis, I will never forget you. Redos. Redos. Redos. Dr. Bruce Reed taught me the beauty of algebra, even though I may never apply it to my work. Dr. Jong Kim taught me the best way to teach is with humor and repetition. He probably doesn't remember his lecture about slicing ellipsoidal forms with a Ginsu knife, but I will never forget it. And, it's true, since his class, I've never seen a bigger "but" on the board.

I would also like to offer a special thank you to the administrative and computer support staff in the Math Department. It's the little things you all have done like reserving rooms, saying hello in the morning, fixing my email, telling me a joke or two, that made it easy to come in everyday and work.

Of course, I cannot forget my husband, Michael, who has got to be the most understanding and forgiving person in the world. You have supported me financially and emotionally throughout this whole graduate school thing and I will never be able to repay you. You really are the most important part of my life and I will never put you second to anything. I love you.

To my parents, thanks for raising me with enough determination to see things through. Mom, thanks for all the encouraging email, especially over the last several months. Dad, thanks for reminding me that I can do anything I set my mind to.

Contents

List of Figures

List of Tables

Chapter 1

Introduction

Throughout history, drops in shear flow have been of interest to many scientists, engineers and mathematicians. In the 1930's, G.I. Taylor, arguably the father of modern fluid mechanics, was particularly interested in the formation of dispersions and emulsions [38, 39]. His empirical experiments laid the foundation for many modern numerically generated comparisons. More recent experimental observations [23, 24, 42] look specifically at sheared breakup in the case of a single drop. Elongative end pinching, retractive end pinching and tip streaming are all processes that yield daughter drops. These theoretical investigations relate directly to the processes of emulsification and mixing which are industrially significant areas of research.

Surfactants can be thought of as small molecules that effect the surface properties of bulk groups of molecules nearby. There are two large classes of surfactants: those that are soluble and those that are insoluble. Soluble surfactants are absorbed into the molecular matrix surrounding them. Insoluble surfactants maintain their independence from the surrounding bulk. We will be examining the effect of insoluble surfactants. In this context, insoluble surfactants can be added to fluid systems deliberately or by chance as impurities, e.g. dust. So, for example, surfactants can be used on purpose to decrease the surface tension between two bulk fluid phases to ease in mixing or emulsification. Similarly, they might fall into mixers or emulsifiers as impurities, but still effect the outcome of the process. It is important to know their effect so that we might accurately predict the outcome of their presence.

1.1 Industrial applications

Most kinds of emulsive mixing lend themselves nicely to a sound understanding of how a surfactant effects a drop exposed to shear flow. In particular, being able to predict drop size and distribution in a product can be most useful for characterizing a variety of material properties including wetting, shear and tear strength or even surface smoothness.

A typical scenario might be to predict the size of paint droplets emitted from a nozzle as they are distributed across an anodized surface. Due to the expense of raw material, if properly controlled, one can maximize paint coverage with minimal thickness. Another scenario might be to predict the distribution of peroxide in a polypropylene matrix during coextrusion. If properly controlled, a new plastic having specific characteristics needed by an engineer, may be created without a chemically reactive process. This too can be a tremendous money and research time saver. Both of these examples represent current and active research projects at public and private research firms.

1.2 Historical interface tracking methods

A problem involving drop dynamics in shear flow is characterized by one significant difficulty, namely how to handle an interface or unknown free boundary within its computational domain. An interface may move within the domain; it may undergo heavy deformation; it may even break. It is therefore necessary to include an interface tracking mechanism in any successful description of such a problem.

Some interface tracking methods include the moving grid method, the front tracking method [41], the level set method and the volume of fluid method [32].

Although the boundary integral method is very accurate in terms of interface reconstruction [52, 43, 50], it does not lend itself to breaking interfaces which is essential to understanding drop breakup and the redistribution of daughter drops or drop fragments. The volume of fluid method does however lend itself nicely to just such a scenario [1, 12, 15].

1.3 Historical work with surfactants

The bulk of the numerical work represented in literature involving insoluble surfactants relates to extensional Stokes flow [9, 43, 52]. Using a boundary integral method to reconstruct interface position and a linear equation of state to represent surfactant concentration, Milliken, Stone and Leal [52] examine the effects of a dilute, insoluble surfactant on the deformation and break-up of viscous drops in two cases: (1) in uniaxial extensional flow and (2) in a surface tension driven motion within a quiescent fluid.

Their problem is best sketched by Figure 1.1. Given a neutrally bouyant drop suspended in an immiscible liquid of infinite extent with a fixed amount of surfactant evenly distributed across the interface, wherein an extensional flow is suddenly applied, they found that surfactants tended to incite three effects: (1) at small viscosity ratios, increased Marangoni stresses cause the drop to behave as if it were more viscous, (2) pointed end caps during drop stretching and (3) more elongated drops before end pinching ensued. The presence of surfactant influenced the flow in two definable ways: (1) a decrease in surface tension

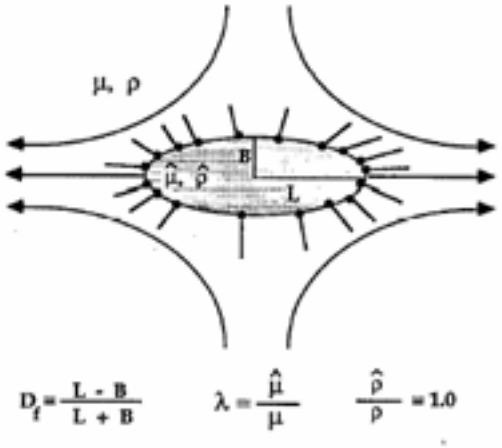

FIG. 1. A sketch of the problem. Not drawn to scale.

Figure 1.1: FIG.1 from [52]. Sketch of drop in extensional flow with insoluble surfactant. Tracking parameters highlighted include D_f = geometric relationship, λ = viscosity ratio, and $\frac{\hat{\rho}}{\rho}$ = density ratio.

at the end caps where surfactant tended to accumulate and (2) a dilution of surfactant concentration as interfacial area increased while the drops stretched.

Milliken et. al. also describe the influence of viscosity ratio coupled with the effect of surfactant pointing out that at large viscosity ratios (>10), surfactant is much less important. However, at viscosity ratio = 1 (where we are also working), they assert that the shape drops maintain (both in stable and unstable formations) is highly dependent on the balance of normal and tangential stresses at the interface. Specifically, normal stresses tend to hold a drop together, whereas, tangential stresses tend to cause necking. They say, "surfactant accumulates along those regions of the interface where the flow converges, lowers the local interfacial tension, and thus requires a higher degree of curvature in order to maintain the normal stress boundary condition." In terms of the physical nature of drop break-up, this relates to the shape of bulbuous ends which will be significant to the shear flow case as well. Figure 1.2 gives a typical drop evolution for the Milliken et. al. study.

Given the case of surface tension driven motion, Milliken et. al. limit their discussion to how surfactants interrelate with Marangoni stresses. For their experiment, they stretch a drop in an extensional flow then instantaneously stop the flow, leaving the extended drop in a quiescent fluid. They note that surfactants have swept to the end areas of the extended

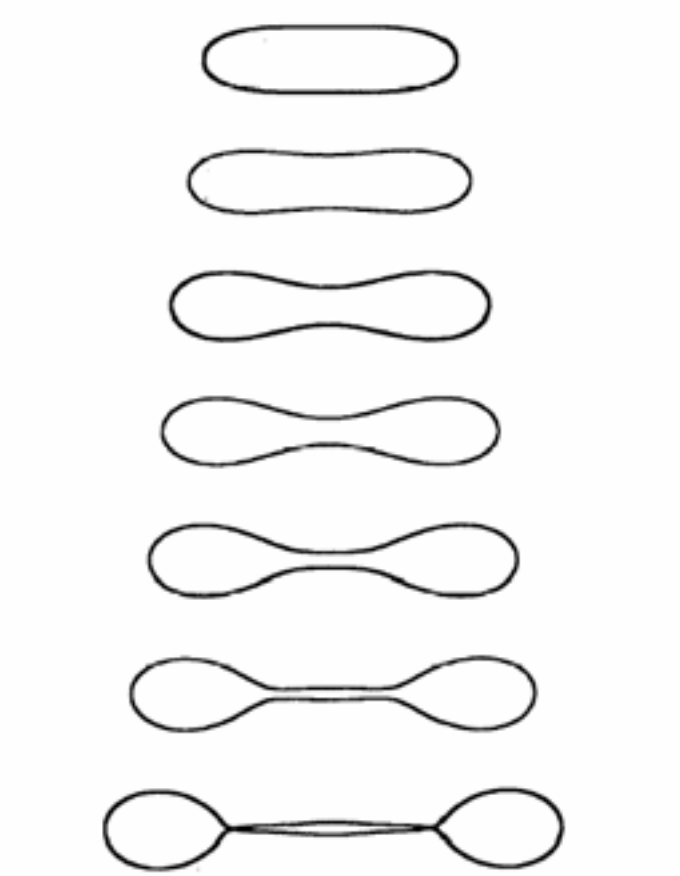

FIG. 6. The stretching of a drop with $\beta=0.95$, $\gamma=10.0$, and $\lambda=1.0$. The simulation is stopped when pinching occurs in the last drawing. The dimensionless times are, reading downward, $t=0$, $t=1201.6$, $t=1265.4$, $t=1289.6$, $t=1305.6$, $t=1313.5$, and $t=1321.5$.

Figure 1.2: FIG.6 from [52]. Drop evolution in extensional flow with insoluble surfactant. Note highly bulbuous ends and very thin neck.

drop. For moderately deformed drops, they report the drop returning to the initial spherical shape. For highly deformed drops, they report the drop undergoes end pinching. They claim that retraction (which is what is expected in the case of no surfactant) is retarded by surfactant location. Marangoni stresses tend to enhance retraction, but the overall reduction in surface tension at the end caps is too high for the drops to recover.

Pawar and Stebe [43] similarly examine axisymmetric extensional flow in the Stokes flow regime at viscosity ratio=1. Unlike Milliken et. al. [52], they implement a non-linear equation of state to represent surfactant concentration. They historically describe a flow without surfactant and indicate that drop shape is determined by viscous stresses that

deform the drop and surface tension that resists deformation. This is typically represented via a capillary number, (Ca), which we use as well.

Pawar and Stebe find essentially the same characteristics in their numerical experiments as do Milliken et.al. They indicate when "flow is initiated, surfactant is swept toward the drop tips, reducing the surface tension there, and altering the interfacial stress balance tangentially through Marangoni stresses and normally through the Laplace pressure." They also convey that surfactant plays a role in tip stretching in the sense that surfactant alters surface tension allowing higher deformation. Similarly, they indicate that as a drop stretches, surface dilution of the surfactant contributes to smaller deformations in the neck area.

One very interesting concept that Pawar and Stebe introduce extends to the chemical nature of surfactants. They relate the molecular structure of a surfactant to the physical phenomena of maximal packing and cohesion. They assert that thinking of surfactant in this manner necessarily mandates the use of a non-linear equation to represent surfactant concentration in order to properly capture surfactant effects related to highly deforming drops. Specifically they say, "surfactant effects on drop deformation are studied in the limit of insoluble surfactant behavior. Surfactants behave as insoluble monolayers in two limits."

There is also limited information available on how surfactants effect stable drops [50, 48] in simple shear flow. (The results are limited to the Stokes flow region.) Yon and Pozrikidis [48] describe a finite volume boundary element method that utilizes a triangular grid to map an evolving fluid interface in the presence of insoluble surfactant. Their results are limited to the stable case and therefore do not extend to the investigation of break up or daughter drop evolution. There is no mention of the physical nature of the flow, and the emphasis of the work is embedded in the associated numerical method. However, the results of the stable case that most closely relate to this work are very good as represented in Figure 1.3.

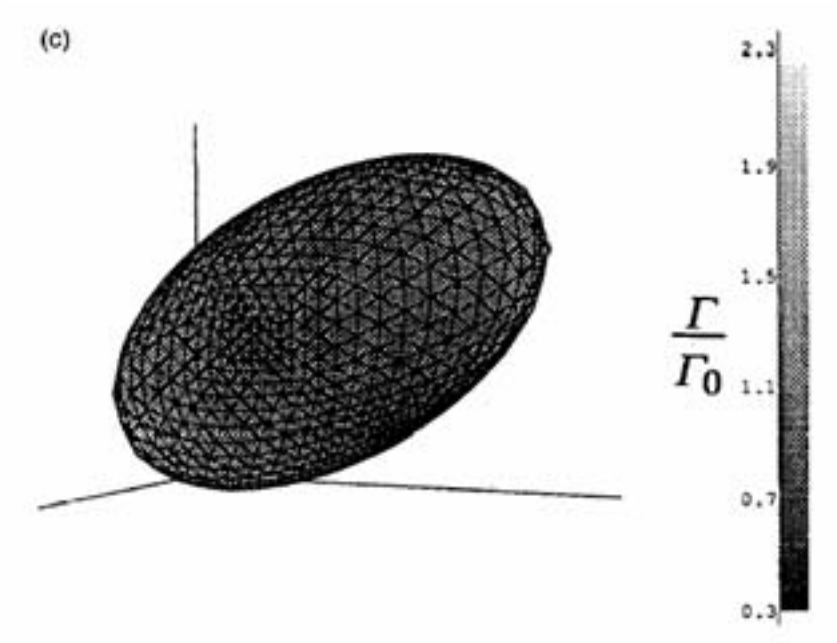

Figure 1.3: FIG.9c from [48]. Stable drop evolution in simple shear flow with insoluble surfactant. Viscosity ratio = 1.0, Stokes flow, Ca=0.25, $\frac{\Gamma}{\Gamma_0}$ = ratio of surfactant concentration.

Li and Pozrikidis [50] describe a boundary element method coupled with a finite difference method for investigating surfactant concentrations over an evolving fluid interface in both extensional and shear flows. Results are limited to the stable case and emphasize the effect of vorticity on surfactants moreso than the effect of surfactant on the flow itself. They treat the surfactant as a "viscoelastic thin shell" and consider the surfactant as acting as a soluble molecular group with an insoluble tail.

Renardy, Renardy and Cristini [15] present a specific 3-dimensional VOF method incorporating surfactant but limit results to low viscosity ratio and the physics of tip streaming. They do, however, formally explain the continuous surface stress formulation (which we use) and implement a linear expression for surfactant concentration (which we also use).

Similarly, de Bruijn [53] gives a nice experimental explanation and depiction of the effect of surfactants on tip streaming and fracture (what we would call break up) in simple shear flow. His modes of drop break up are physically experimental, not numerically predictable, but are generally similar to the results generated for this paper as can be seen in Figure 1.4.

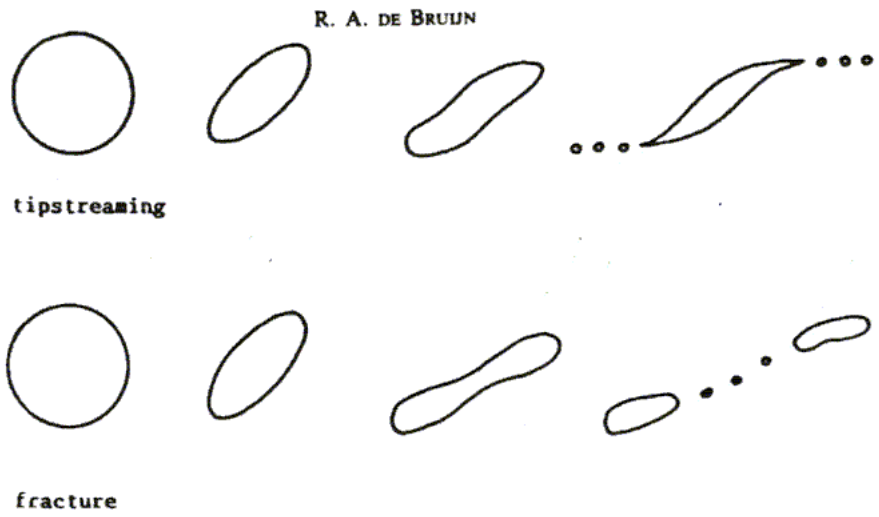

Figure 1.4: FIG.1 from [53]. Modes of drop break-up observed in experimental simple shear flows.

1.4 Importance of this work

The material presented in this dissertation is a culmination of numerical code [1, 15] with the physical necessity of understanding the fracture breakup mode of droplets in shear flow [53] under the effect of surfactant. We investigate the fracture breakup mode described by DeBruijn in the neighborhood of drop to matrix viscosity ratio = 1.

This dissertation is divided into several chapters. Chapter 2 is a description of the numerical method used. Chapter 3 offers basic results of stable and unstable drop evolution under the effect of an insoluble surfactant. Chapter 4 gives the critical curve which represents the threshold between stable and unstable drops in shear flow with surfactant. Chapter 5 investigates the effect surfactant has on the evolution of daughter drops. Chapter 6 is a numerical verification of data.

Chapter 2

Numerical Method

2.1 SURFER++

SURFER++ [15, 14, 34, 1] is composed of 3 parts. The first is a volume of fluid (VOF) method that tracks the interface [32, 2] which is based on a piecewise linear interface construction (PLIC)[30, 2], a projection method to solve the Navier-Stokes equations on the MAC grid [31, 35], and a continuum method for modeling interfacial tension [15].

2.1.1 The equations of motion for a drop in shear flow

The flow is composed of two immiscible liquids of different densities and viscosities. The density (ρ) and viscosity (μ) of each fluid is constant in each particular fluid. In the configuration considered in this work specifically, a single sphere is suspended centrally in a box-shaped computational domain. Shear is imposed by considering that the top and bottom sections of the box move with some velocity in opposite but parallel directions. See Figure 2.1. A concentration function (C) is used to track the interface. Particularly,

$$C = \begin{cases} 1, & \text{fluid 1} \\ 0, & \text{fluid 2.} \end{cases} \tag{2.1}$$

C is transported by the velocity field $\mathbf{u}$:

$$\frac{\partial C}{\partial t} + \mathbf{u} \cdot \nabla C = 0. \tag{2.2}$$

The average values of ρ and μ are interpolated as:

$$\rho = C\rho_1 + (1 - C)\rho_2, \tag{2.3}$$

$$\mu = C\mu_1 + (1 - C)\mu_2, \tag{2.4}$$

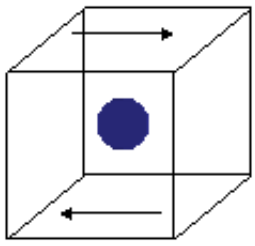

Figure 2.1: Generalized problem of a drop in shear flow

where the subscripts refer to fluid 1 or fluid 2. The flow satisfies the incompressibility condition,

$$\nabla \cdot \mathbf{u} = 0. \tag{2.5}$$

And, the flow is governed by the Navier-Stokes equation:

$$\rho(\frac{\partial \mathbf{u}}{\partial t} + \mathbf{u} \cdot \nabla \mathbf{u}) = -\nabla p + \nabla \cdot \mu \mathbf{S} + \mathbf{F} \tag{2.6}$$

where $\mathbf{S}$ is the viscous stress tensor,

$$\mathbf{S} = \frac{1}{2}(\nabla \mathbf{u} + (\nabla \mathbf{u})^T), \tag{2.7}$$

and $\mathbf{F}$ is the body force which includes both the gravity and interfacial tension forces. The interfacial tension force ($\mathbf{F}_s$) is defined as:

$$\mathbf{F}_s = \sigma \kappa \mathbf{n}_s \delta_s, \tag{2.8}$$

where σ is interfacial tension, κ is mean curvature and $\mathbf{n}_s$ is the normal to the interface.

2.1.2 The VOF method and PLIC

The concentration function, C, of Equation 2.1 can be thought of as a scalar volume fraction field. $0 < C < 1$ in cells cut by the interface and $C = 0$ or $C = 1$ away from it. C is known at the beginning of each computational cycle, but it does not discretely give the position of the interface. To approximate this location, an estimate of the normal vector ($\mathbf{n}_s$) at the interface is also required. See Figure 2.2.

The approximate normal to the interface in each cell is equal to the discrete gradient of the volume fraction field. Specifically,

$$\mathbf{n}_s = \frac{\nabla C}{|\nabla C|}. \tag{2.9}$$

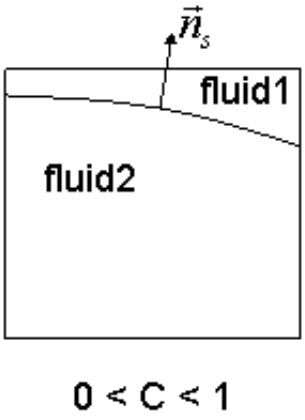

Figure 2.2: Visualizing concentration function: an example of a 2-dimensional cell cut by an interface

Having this information, a planar surface is constructed within each interfacial cell having the same normal and dividing the cell into two parts [2]. See Figure 2.3. Each part of the cell discretely contains the proper volume of each fluid. The planar interface representation

Construct Interface Approximation in single cell

Update Interface Position across neighboring cells

Figure 2.3: Visualizing PLIC: an example of a 2-dimensional construction

is then propagated by the flow and the resulting mass, momentum and volume fluxes of each fluid are determined in neighboring cells using a Lagrangian advection method [30]:

$$\mathbf{x}^{n+1} = \mathbf{x}^n + \mathbf{u}(\Delta t). \tag{2.10}$$

Values of the volume fraction, mass and momentum fields are calculated throughout the computational domain and the simulation proceeds to the next time step.

2.1.3 The projection method

Solving the Navier-Stokes equation is computationally expensive. An efficient approximation has been documented by [35] and proceeds as follows. Starting at time level n, an intermediate velocity $\mathbf{u}^*$ is calculated to satisfy:

$$\frac{\mathbf{u}^* - \mathbf{u}^n}{\Delta t} = -\mathbf{u}^n \cdot \nabla \mathbf{u}^n + \frac{1}{\rho}(\nabla \cdot (\mu \mathbf{S}) + \mathbf{F})^n. \tag{2.11}$$

Generally speaking, $\mathbf{u}^*$ is not divergence free. It must be corrected by the pressure term

$$\frac{\mathbf{u}^{n+1} - \mathbf{u}^*}{\Delta t} = -\frac{\nabla p}{\rho}, \tag{2.12}$$

where $\mathbf{u}^{n+1}$ at time level$n + 1$ satisfies the incompressibility condition:

$$\nabla \cdot \mathbf{u}^{n+1} = 0. \tag{2.13}$$

Substituting Equation 2.12 into Equation 2.13 results in a Poisson equation for the pressure

$$\nabla \cdot (\frac{\nabla p}{\rho}) = -\frac{\nabla \cdot \mathbf{u}^*}{\Delta t}. \tag{2.14}$$

The solution of this equation is the most time consuming part of the solver. It is approached with a multi-grid method composed of one iterative method to reduce high frequency error, and one coarse grid correction to eliminate low-frequency error. The weakness of the above characterization is that is an explicit method and not suitable for simulations at low Reynolds number. [1] gives a semi-implicit scheme which is unconditionally stable for all Re in this paper.

2.1.4 Modelling interfacial tension

There are two dominant methods for modelling interfacial tension. The first is the continuous surface force (CSF) formulation [28]. The second is the continuous surface stress (CSS) formulation [29]. In both cases, interfacial tension force is defined as in Equation 2.8:

$$\mathbf{F}_s = \sigma \kappa \mathbf{n}_s \delta_s. \tag{2.15}$$

where

$$\nabla C = \frac{\mathbf{n}_s}{\delta_s} \tag{2.16}$$

Both methods are equivalent at the continuum level. In CSF, because the concentration function, C, is discontinuous at the interface, it is replaced by a smoothed function, $\tilde{C}(x)$, which varies continuously from 0 to 1 over a distance defined by the order of the mesh, O(ϵ). ϵ is chosen specifically to be twice the mesh size. $\tilde{C}$ is calculated by convolving the original concentration function, C with a kernel function, $\mathbf{K}(x, \epsilon)$:

$$\mathbf{K}(x, \epsilon) = \int_\Omega C(x')\mathbf{K}(x' - x, \epsilon)dx'. \tag{2.17}$$

Specifically, SURFER++ uses the kernel function, $\mathbf{K}_8$ from [36]. $\tilde{C}$ is calculated with two smoothing steps so that spurious currents related to inaccurate discrete approximations of $\mathbf{n}_s$ and κ are suppressed. In CSS, no smoothing of the concentration function takes place. This avoids any duffusion of the surface tension force, hence there is minimal "numerical" surfactant, i.e. removing the smoothing component reduces error in the surfactant case.

2.2 Incorporating surfactant

Having given a generalized method for solving the problem of a single drop in shear flow, the question becomes how to include a surfactant layer in the method. This has been addressed in [15] and will be summarized here.

We choose the CSS method with no smoothing to model the interfacial tension force, with the exception that now interfacial tension, σ, is non-constant because of the addition of surfactant. We can equivalently rewrite the interfacial tension force, $\mathbf{F}_s$, of Equation 2.15 as follows:

$$\mathbf{F}_s = \nabla \cdot \mathbf{T} \tag{2.18}$$

where $\mathbf{T}$ is surface stress:

$$\mathbf{T} = [(\mathbf{1} - \mathbf{n}_s \otimes \mathbf{n}_s)\sigma\delta_s]. \tag{2.19}$$

The idea is modify $\mathbf{T}$ to replace σ with $\sigma - E\Gamma$, where E is an elasticity number that is a measure of the sensitivity of the surface tension to the surfactant concentration, Γ, as explained in [9]. Mathematically speaking, $\sigma - E\Gamma$ represents the linear equation of state for surfactant concentration. Because the VOF method requires the use of volumes rather than surface information, an additional two spheres are added to the geometric definition of the problem. One sphere is interior to the original drop with radius $\frac{h}{2}$ smaller. The other sphere is exterior to the original drop with radius $\frac{h}{2}$ larger. Specifically, h is a prespecified thickness of surfactant. See Figure 2.4. We define the VOF functions, c_+ and c_- in the outer and inner spheres respectively. Specifically,

$$c_+ = \begin{cases} 1, & \text{inside outer sphere} \\ 0, & \text{outside outer sphere} \end{cases} \tag{2.20}$$

and

$$c_- = \begin{cases} 1, & \text{inside inner sphere} \\ 0, & \text{outside inner sphere.} \end{cases} \tag{2.21}$$

The surfactant lives between the inner and outer spheres, and Γ is a constant multiple of $c_+ - c_-$ which equals 1 in the spherical annulus between the constructed spheres and 0 outside. All three interfaces are tracked during the numerical simulation. Reconsidering Equation 2.19, the $\sigma\delta_s$ term is replaced by $\sigma|\nabla C| - K(c_+ - c_-)$. Upon integration from the inner to the outer sphere in the radial direction, this expression becomes $\sigma - Kh$. Recalling

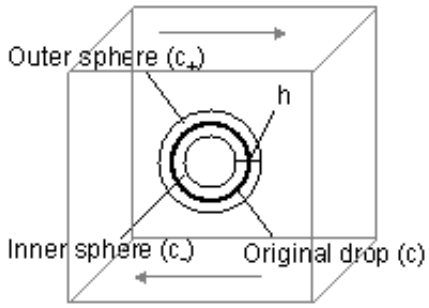

Figure 2.4: Generalized problem of a drop in shear flow including surfactant

that surface tension has been predefined as variable in the sense that it is represented by $\sigma - E\Gamma$, it is obvious that $Kh = E\Gamma$. So:

$$\mathbf{T} = (\mathbf{1} - \mathbf{n}_s \otimes \mathbf{n}_s)[\sigma|\nabla C| - \frac{E\Gamma}{h}(c_+ - c_-)]. \tag{2.22}$$

Furthermore, we specify a reduction factor, r, which is most easily thought of as a theoretical change in the surface tension of the drop caused by the addition of surfactant. Specifically,

$$r = \frac{E\Gamma}{\sigma} = 1 - \frac{\text{surface tension with surfactant}}{\text{surface tension without surfactant}}. \tag{2.23}$$

Using simple algebraic manipulation, it is easy to see that $K = \frac{\sigma r}{h}$. Both r and h are input parameters.

2.3 Other important parameters

There are several different dimensionless parameters used in the simulations. The ones most important to understanding the data presented in the results include capillary number, effective capillary number and Reynolds number. Capillary number (Ca) is defined as

$$Ca = \frac{a\dot{\gamma}\mu_m}{\sigma} \tag{2.24}$$

where $\dot{\gamma}$ is an average shear rate defined over plate separation distance. Recall a is the radius of the drop, μ is viscosity, and σ is surface tension. The subscript m refers to the matrix fluid (i.e. outside the drop). Capillary number can be thought of as a measure of the viscous force causing deformation relative to interfacial tension force which keeps a drop together.

Because of its definition, capillary number changes reflect distinct changes in surface tension which is a key idea in surfactant simulation. Effective capillary number (Ca_e) is defined as

$$Ca_e = \frac{a\dot{\gamma}\mu_m}{\sigma_e} = \frac{a\dot{\gamma}\mu_m}{\sigma(1-r)} = \frac{Ca}{1-r} \tag{2.25}$$

where r refers to reduction as defined in Equation 2.23. Reynolds number (Re) is defined by

$$\mathrm{Re} = \frac{\rho_m \dot{\gamma} a^2}{\mu_m} \tag{2.26}$$

where ρ is density. Reynolds number is often the focus of studies involving changes in viscosity. Generally speaking, it is best to remember that low Reynolds number indicates a high viscosity (think thick). High Reynolds number indicates low viscosity (think runny).

2.4 Parallelization

The numerical scheme has been entirely parallelized as described in [40]. The code runs on an Origin2000. In total, we have used as many as 8 multiple processors and 774 megabytes of physical memory. A scalability study was conducted on the specific case of Re=10, Ca=0.14, r=0.1, computational box size = 2 x $\frac{1}{2}$ x 1, spatial mesh = $\frac{1}{64}$, and time step = $10^{-3}s$. For each test, CPU time was recorded for 1000 time steps. Figure 2.5 illustrates a somewhat exponential relationship between number of processors and time to calculate a 1 second progression in the numerical simulation.

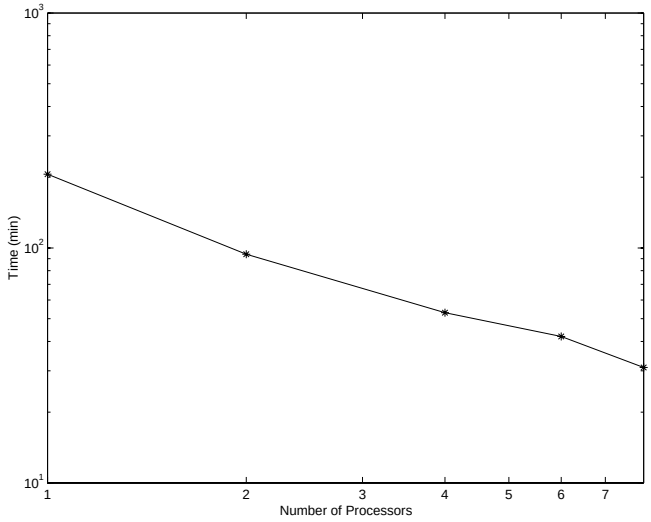

Figure 2.5: Scalability of Surfer++ with surfactant addition. Specific Run used for study: Re=10, Ca=0.14, r=0.1, Computational box size = 2 x $\frac{1}{2}$ x 1, Spatial mesh = $\frac{1}{64}$, Time step = $10^{-3}s$. Time shown represents machine time to calculate a 1 second progression of simulation.

Speed-up factors are defined as the time it takes an operation to be conducted on a single processor divided by the time it takes an operation to be conducted on a multiple number of processors. Table 2.1 and Figure 2.6 illustrate this idea for the previously described scalability study.

Processors	CPU Time (min)	Speed-up factor
1	206	1.0
2	94	2.2
4	53	3.9
6	42	4.9
8	31	6.6

Table 2.1: CPU time for 1000 time steps in a 3D simulation of drop break up with surfactant

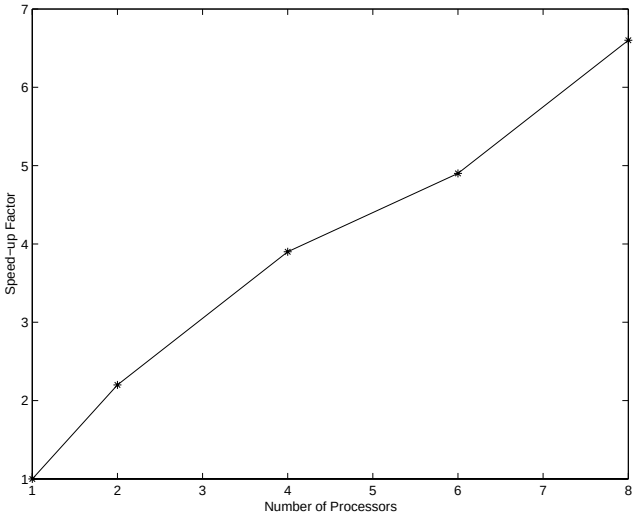

Figure 2.6: Speed-up factor curve for 3D simulation of drop break up with surfactant on up to 8 processors

Code efficiency is defined as the ratio $\frac{\text{CPU time on N processors}}{\frac{\text{M}}{\text{N}}\text{x CPU time on M processors}}$. Table 2.2 illustrates efficiency ratings of interest.

From N Processors	To M Processors	Efficiency (%)
1	2	109
1	4	97
1	6	82
1	8	86
2	4	89
2	8	75
4	6	84
4	8	85
6	8	102

Table 2.2: Efficiency ratings for various CPU count changes of 3D simulation of drop break up with surfactant

Chapter 3

Effect of Surfactant on Drop Evolution

3.1 Numerical Presets

All data presented in this chapter are generated using a $\frac{1}{64}$ mesh. The computational box size, however, varies with Reynolds number. For Re $\leqslant$ 1.5, the computational box size is 2 x $\frac{1}{2}$ x 1. For Re $>$ 1.5, the computational box size is 3 x $\frac{1}{2}$ x 1. The different box sizes are necessary to capture break-up sequences without neighboring drops interfering with the calculations.

In all cases, a matrix to drop viscosity ratio of 1.0 is maintained. Similarly, density is matched inside and outside the drop. The effect of reduction factor is evaluated at $r = 0.1$, but higher reduction factor levels from 0.2 to 0.4 are evaluated in some simulations. Recall that r represents a theoretical change in the surface tension of a drop caused by the addition of surfactant. See Equation 2.23. Note that a reduction equal to 0 is equivalent to the case of no surfactant.

The surfactant layer between the drop and matrix phases is equal in thickness to $\frac{1}{50}$th of the numerical mesh.

3.2 Stable drop evolution

In the case of a steady-state solution, when a drop of viscous liquid is placed in a matrix liquid of equal viscosity and subsequently sheared, we expect the motion to result in an ellipsoidal shape. We investigate steady-state drop evolution in a similar circumstance whereby we have added a layer of surfactant between the drop and matrix liquids.

3.2.1 Results

The addition of surfactant causes stable drops to be (1) more elongated and (2) less inclined against the primary flow direction. The geometry of these effects is described in terms of the deformation parameters half-length/radius (L/a) and the angle of inclination that the drop takes with the horizontal (θ) as in [1]. See Figure 3.1.

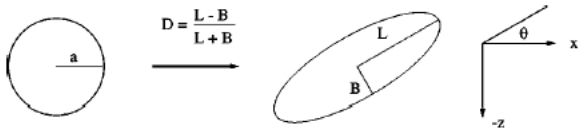

FIG. 4. Scalar measures of deformation and orientation.

Figure 3.1: Drop deformation parameters. Reproduction of Figure 4 from [1]

Table 3.1 illustrates a typical change in deformation parameters upon the addition of surfactant at $r = 0.1$ for a stable evolution at Re=10. To reiterate, surfactant causes a stable drop to be more elongated (L/a increases) and less inclined (θ decreases) against the primary flow direction.

r	Ca	Ca_e	L/a	θ (°)
0	0.15	0.150	1.59	35.0
0.1	0.13	0.144	1.63	29.9

Table 3.1: Typical deformation parameters for stable drop evolution,Re=10, r=0, 0.1

Figure 3.2 illustrates the physical appearance of the two drops from Table 3.1 evolving into stable shapes. The progression on the left side has no surfactant; the progression on the right side has surfactant. From top to bottom, the time step between each picture is 1 second. Time steps are matched from left to right. Initially the drop is a sphere. When the shear flow begins the drop elongates then eventually stabilizes to a somewhat ellipsoidal form. This sequence of events is generally true with or without surfactant, but as evident in Table 3.1 the deformation parameters vary between the two cases.

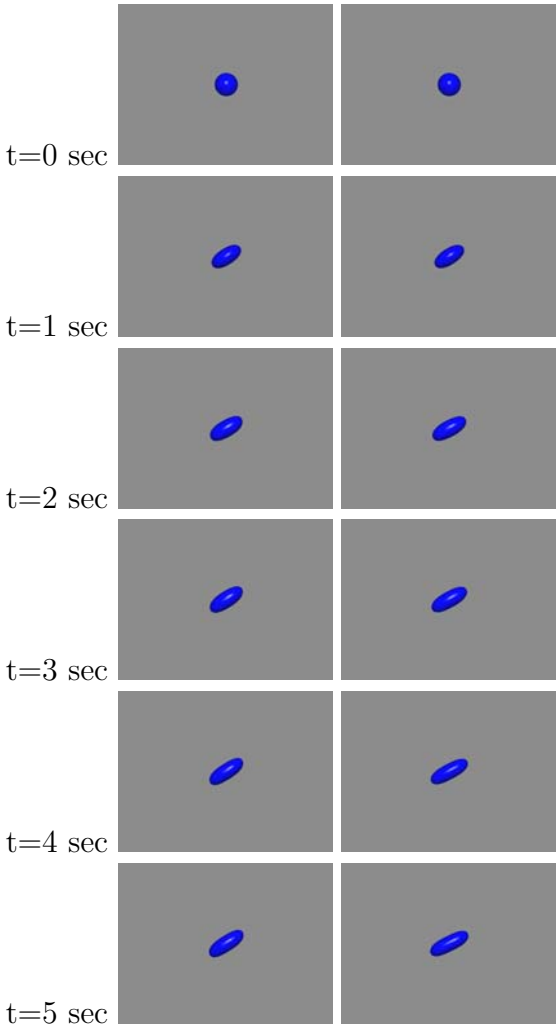

Figure 3.2: Comparison of stable drop evolution at Re=10, Left: r=0; Right: r=0.1

The location of the surfactant during the simulation of Figure 3.2 explains the change in deformation parameters from the no-surfactant case. Recall that surfactant lowers the surface tension of the interface in its local area. As you can see in Figure 3.3, the surfactant tends to migrate to the end caps of the drop.

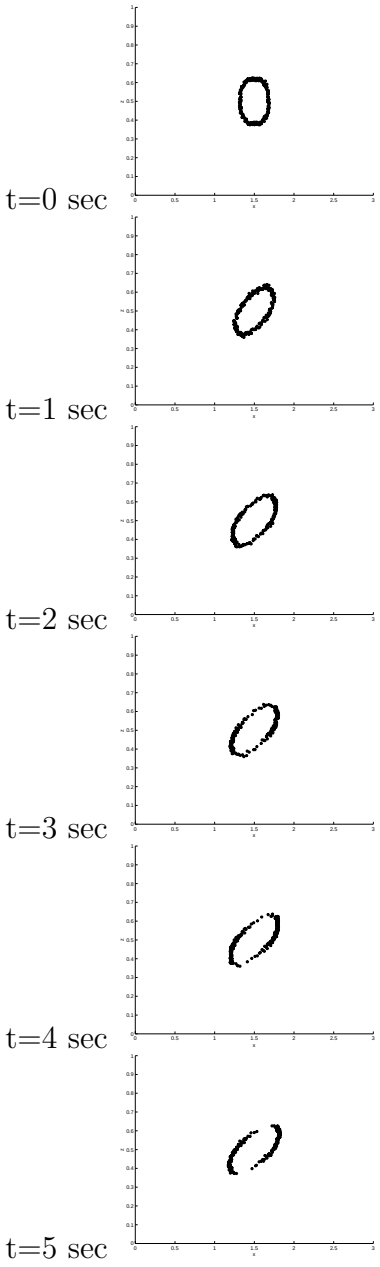

Figure 3.3: Surfactant Migration over time in stable drop. Re=10, Ca=0.13, Ca_e=0.144, r=0.1

The motion of the surfactant to the end caps reduces the surface tension in that local area. This allows the flow interior to the drop to push the end caps out, thus slightly elongating the drop. The elongation also results in a change in the velocity field of the flow interior to the drop. A much larger vertical component explains the less inclined configuration of the surfactant coated drop. If one examines the velocity fields of the flow near the interface, it is easier to see the nature of this effect. See Figure 3.4. One can also see that the circulation pattern within the drops is different. When no surfactant is present, the stable drop on the left has two centers of circulation, near the end caps. When surfactant is present, the stable drop on the right has a single center of circulation, further indicative of the lower θ value. When a drop lays more in line with the flow direction, less inertial force is exerted on the fluid inside the drop near its end caps. Inertial force is translated to fluid motion inside the drop. As the angle of inclination increases, the inertial force increases at the end caps resulting in two circulation centers instead of one.

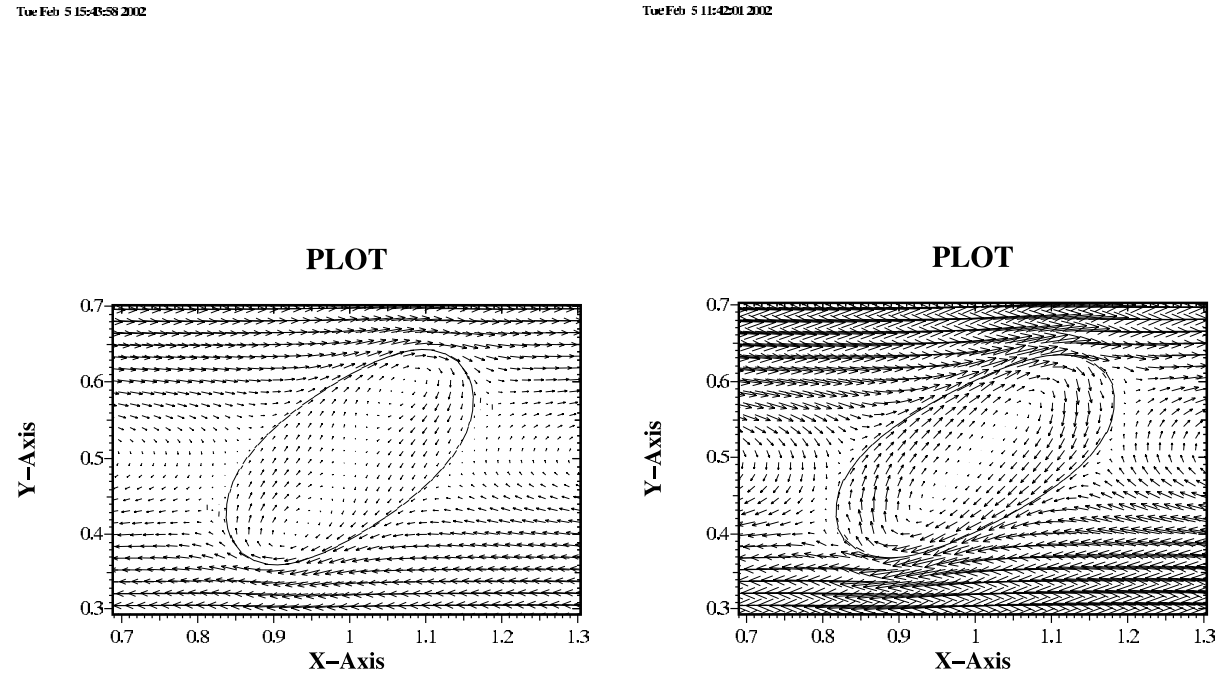

Figure 3.4: Velocity Fields for Stable Drop Configuration, Re=10. Left: $r = 0$, Right: $r = 0.1$

Furthermore, Marangoni stresses acting along the drop interface tend to keep the angle low. Pawar and Stebe [43] specifically define the Marangoni stress as

$$Ma = \frac{\delta\sigma}{\delta\Gamma}\nabla_S\Gamma, \tag{3.1}$$

where σ is interfacial tension and Γ is surfactant concentration. This indicates that in areas where surface tension is changing rapidly, a large Marangoni stress works against the drop in the flow direction. This correlates to areas along the drop interface where surfactant

accumulates locally next to an area where there is no surfactant. The last picture of Figure 3.3 indicates that this phenomenon occurs most strongly near both end caps of the drop, thus further aligning the drop with the flow.

This study incorporates an investigation of stable drop evolution for the range of Reynolds numbers $0.2 \leqslant \mathrm{Re} \leqslant 100$. Table 3.2 iterates the deformation parameters exhibited by drops in this range upon the addition of surfactant. When data is available, a comparison between r=0 and r=0.1 is given. Aside from Re<1, we still see that the addition of surfactant at the level of reduction, r=0.1, results in more elongated drops with less angular inclination. The shorter drops seen at Re<1 can best be explained by a result found in [52]. Milliken et.al.'s conclusion for extensional flow extends to the shear flow case. They say, "surfactant accumulates along those regions of the interface where the flow converges, lowers the local interfacial tension, and thus requires a higher degree of curvature in order to maintain the normal stress boundary condition." The higher degree of curvature tends to shorten the drops in this flow regime. Similarly, "gradients in surfactant concentration also retard the interfacial velocity and cause the drop to appear more viscous" than it actually is.

We also note that as we hold reduction constant at r=0.1, and increase Re, the drops become less elongated, flatter at the end caps and more highly inclined. This makes sense. Low Re indicates more viscous forces are at work, which tends to add to elongation. High Re indicates more inertial forces are at work, which tends to add to angular inclination. Figures 3.5, 3.6, 3.7, and 3.8 represent the velocity fields of the stable drops over the full spectrum of Re evaluated in this study at r=0.1 and iterated in Table 3.2.

Re	Ca	Ca	Ca_e	L/a	L/a	θ (°)	θ (°)
	r=0	r=0.1		r=0	r=0.1	r=0	r=0.1
0.2	0.36	0.31	0.344	2.59	2.07	20.5	18.1
0.2	0.344	0.31	0.344	1.98	2.07	18.6	18.1
0.4	0.33	0.29	0.322		2.06		17.8
0.6	0.31	0.27	0.300		1.99		22.2
0.8	0.29	0.26	0.234	1.95	2.13	24.0	21.4
1.0	0.27	0.24	0.267	1.76	2.13	27.5	26.0
1.25	0.26	0.235	0.261	1.80	1.92	25.2	24.5
1.5	0.25	0.225	0.250	1.79	1.91	24.8	24.3
2.0	0.24	0.21	0.233	1.81	1.87	27.6	25.7
3.0	0.21	0.19	0.211	1.65	1.84	32.7	25.8
4.0	0.20	0.17	0.188		1.66	34.0	32.6
6.0	0.18	0.15	0.167		1.62		29.7
10.0	0.15	0.13	0.144	1.59	1.63	35.0	29.9
15.0	0.125	0.11	0.122		1.69		30.0
21.0	0.105	0.09	0.100		1.50		31.8
25.0	0.095	0.08	0.089		1.47		38.1
40.0	0.070	0.067	0.074		1.47		38.1
50.0	0.061	0.056	0.062	1.52	1.52	48.3	41.6
60.0	0.053	0.052	0.057		1.52	48.0	41.6
80.0	0.041	0.042	0.046		1.86		42.2
100.0	0.032	0.037	0.041		1.81		42.0

Table 3.2: Comparative L/a and θ for r=0 and r=0.1 over $0.2 \leqslant \mathrm{Re} \leqslant 100$

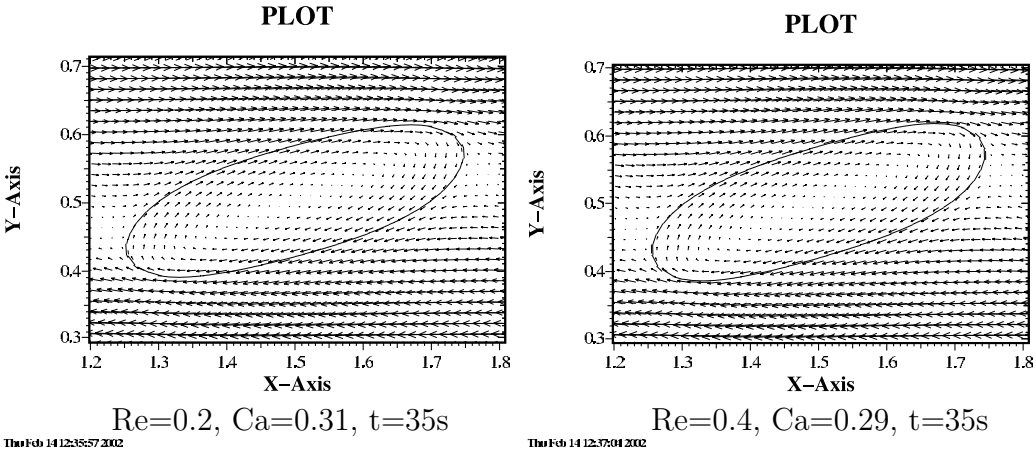

Re=0.2, Ca=0.31, t=35s Re=0.4, Ca=0.29, t=35s

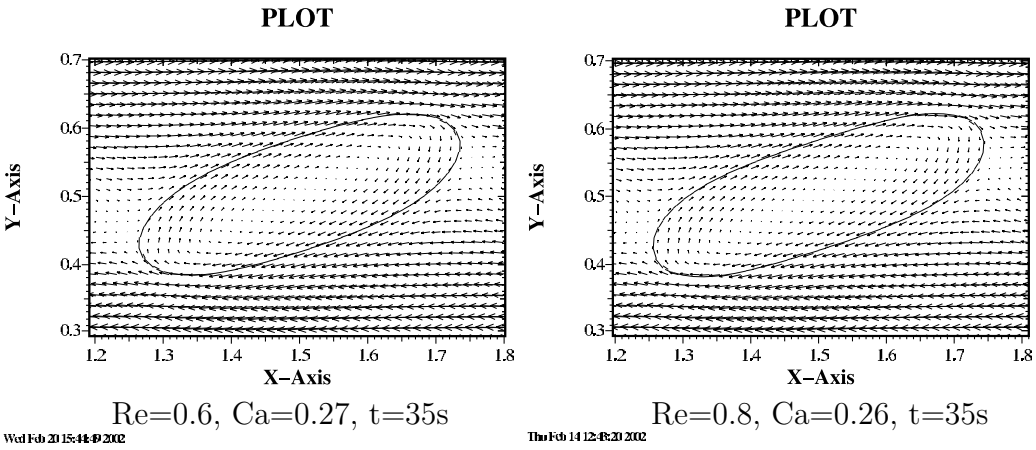

Re=0.6, Ca=0.27, t=35s Re=0.8, Ca=0.26, t=35s

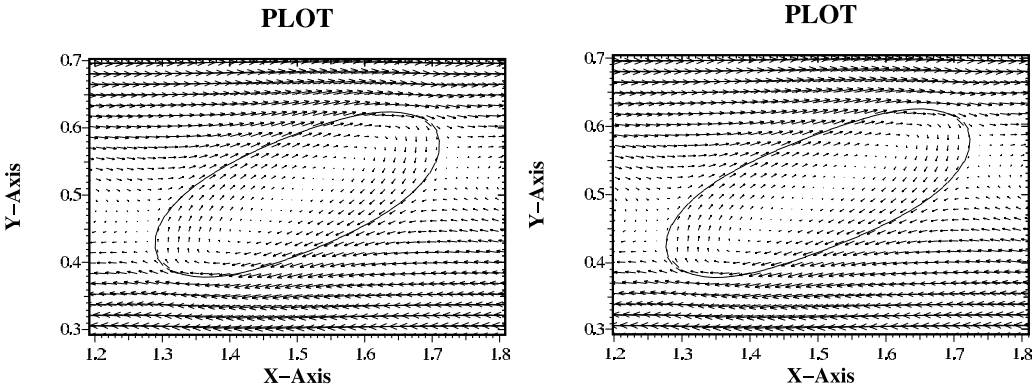

Re=1.0, Ca=0.24, t=35s Re=1.25, Ca=0.235, t=24s

Figure 3.5: Stable drops at r=0.1, $0.2 \leqslant \mathrm{Re} \leqslant 1.25$

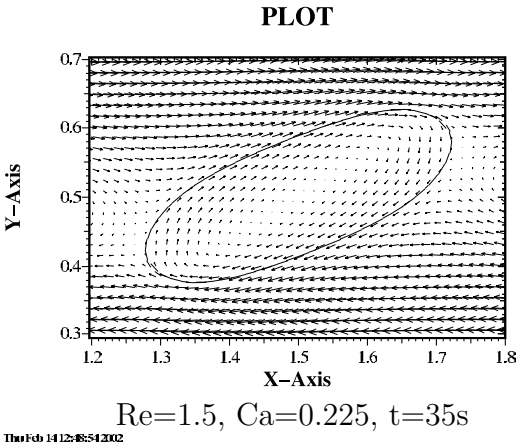

Re=1.5, Ca=0.225, t=35s

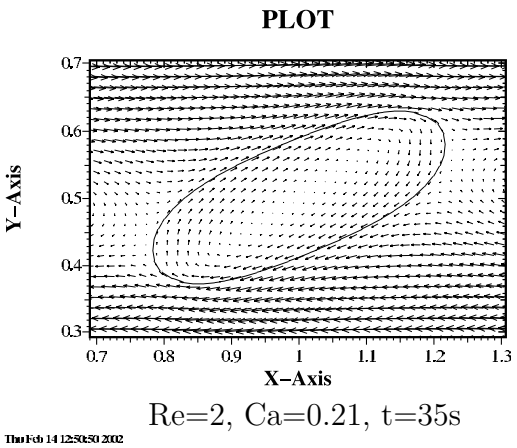

Re=2, Ca=0.21, t=35s

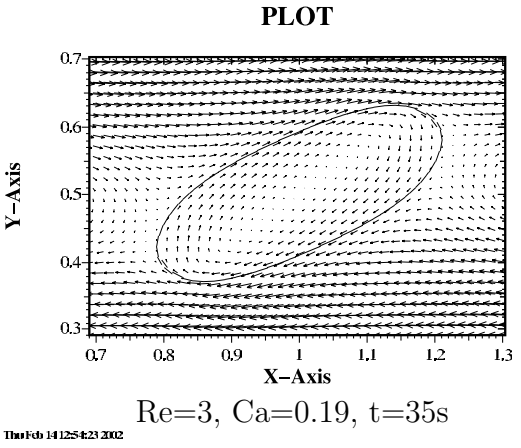

Re=3, Ca=0.19, t=35s

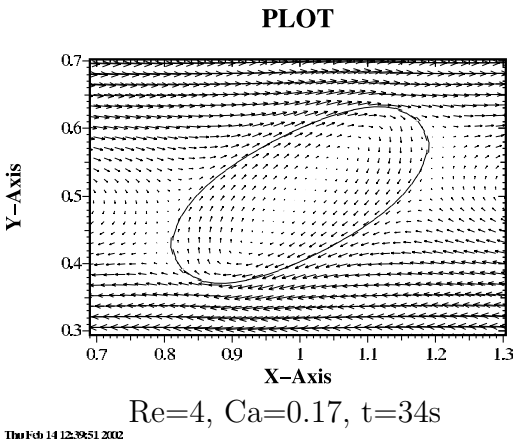

Re=4, Ca=0.17, t=34s

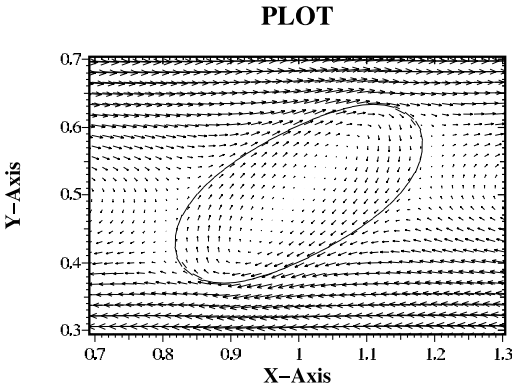

Re=6, Ca=0.15, t=24s

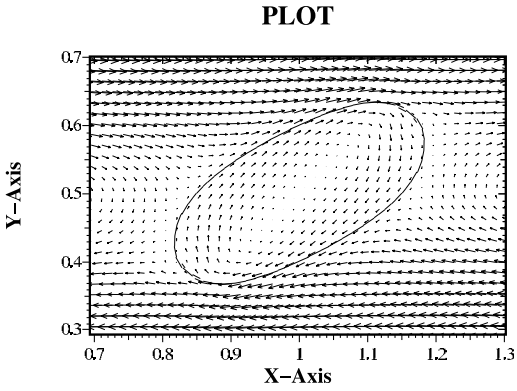

Re=10, Ca=0.13, t=35s

Figure 3.6: Stable drops at r=0.1, $1.5 \leqslant \mathrm{Re} \leqslant 10$

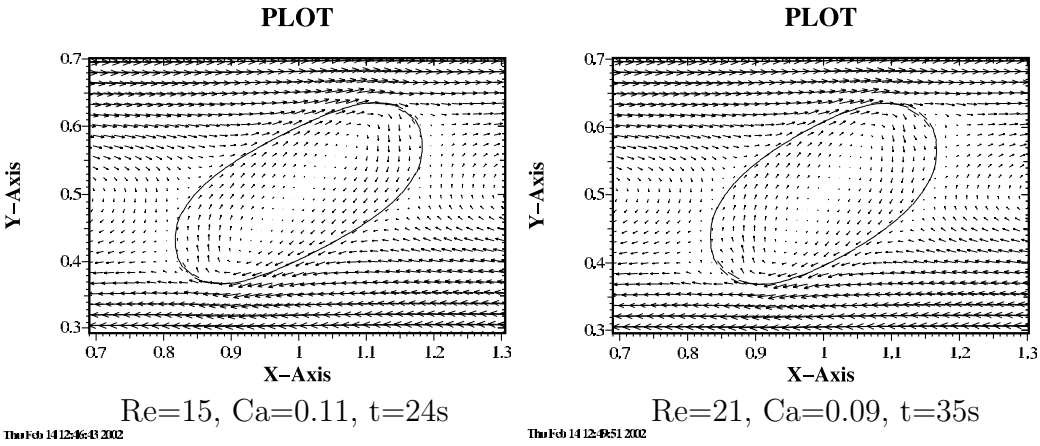

Re=15, Ca=0.11, t=24s Re=21, Ca=0.09, t=35s

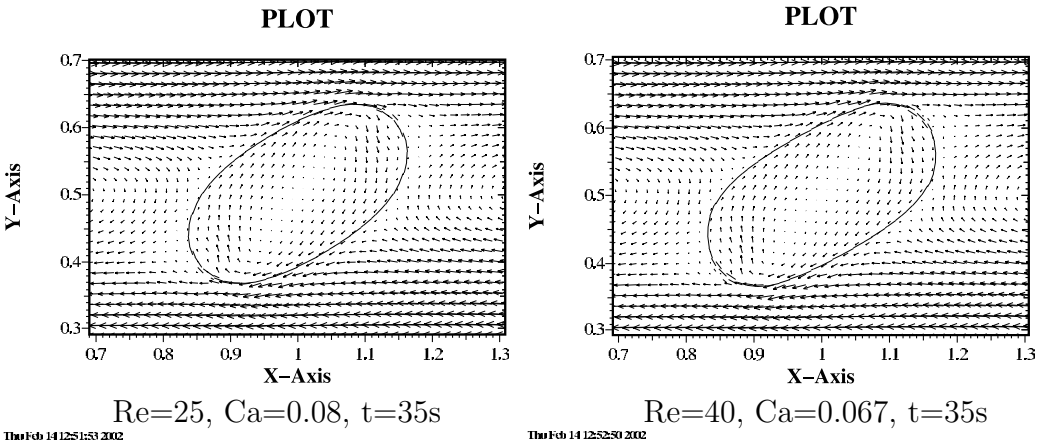

Re=25, Ca=0.08, t=35s Re=40, Ca=0.067, t=35s

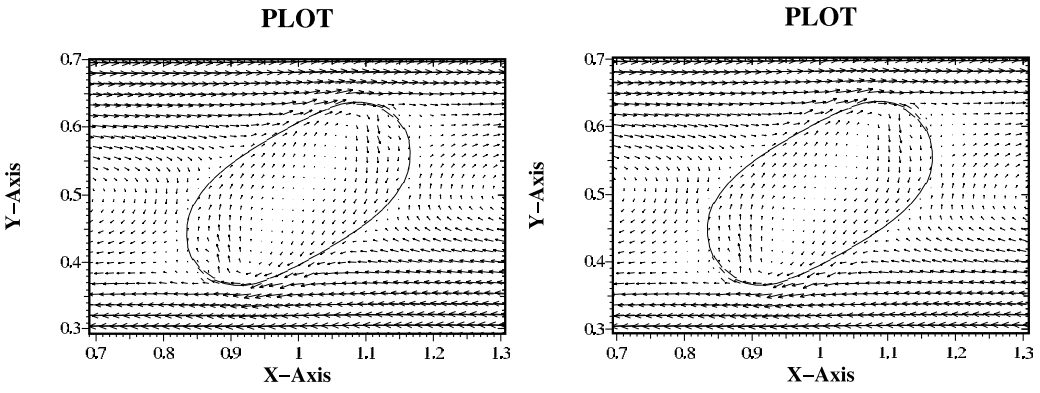

Re=50, Ca=0.056, t=24s Re=60, Ca=0.052, t=35s

Figure 3.7: Stable drops at r=0.1, $15 \leqslant \mathrm{Re} \leqslant 60$

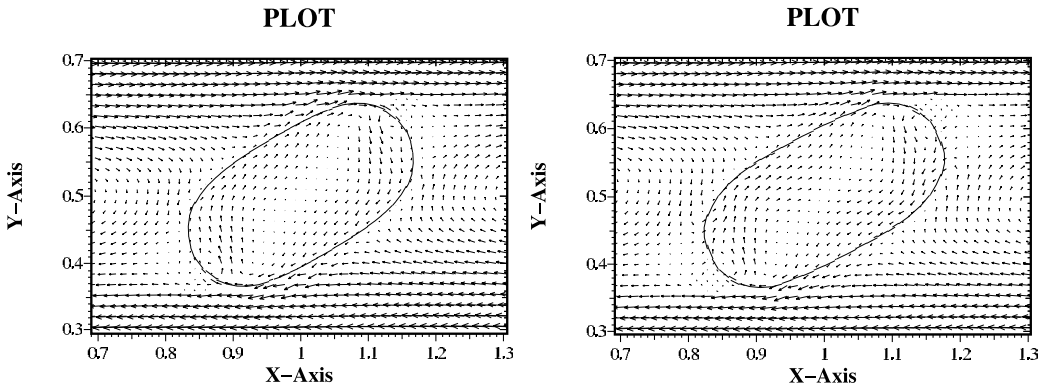

Re=80, Ca=0.042, t=30s Re=100, Ca=0.037, t=35s

Figure 3.8: Stable drops at r=0.1, $80 \leqslant \mathrm{Re} \leqslant 100$

3.2.2 Higher levels of reduction

As reduction increases, we see two different trends emerge. For low Reynolds number (here represented by Re=1), we see that the drops continue to elongate and lower their angle of inclination with the flow. At higher Reynolds number (here represented by Re=50 and 60), we see that an increase in reduction results in less drop elongation and a stabilization of the angle of inclination. See Table 3.3. These trends are consistent with the physical nature of the problem. At low Reynolds number, viscous forces are higher and surfactant tends to sweep to the end caps of the drops even as surface tension is reduced. At higher Reynolds number, inertial forces dominate and surfactant tends to stagnate as surface tension is reduced. See Figures 3.9 and 3.10. Stagnation can best be thought of as areas where the velocity of the flow is equal to zero. Some refer to these areas as 'dead spots' in the flow. These stagnation points coincide with areas where Marangoni stresses (as explained in Section 3.2.1 and Equation 3.1) are highest and therefore where the largest concentration of surfactant is present. The drops and surfactant have coincidentally achieved equilibrium. The drops have stabilized to a discrete shape and the surfactant coating them has also stopped migrating.

Re	r	Ca	Ca_e	L/a	θ (°)
1	0	0.27	0.270	1.76	27.5
	0.1	0.24	0.267	2.13	26.0
	0.2	0.21	0.263	1.92	20.9
	0.3	0.18	0.257	2.14	18.7
	0.4	0.15	0.250	2.28	17.5
50	0	0.061	0.061	1.52	48.3
	0.1	0.056	0.062	1.52	41.6
	0.2	0.047	0.058	1.36	41.3
	0.3	0.036	0.051	1.37	41.4
	0.4	0.029	0.048	1.41	42.0
60	0	0.053	0.053		
	0.1	0.052	0.057	1.52	41.6
	0.2	0.041	0.051	1.50	41.6
	0.3	0.031	0.044	1.36	41.5
	0.4	0.026	0.043	1.37	42.0

Table 3.3: Comparison of stable drop evolution under different levels of reduction, Re=1, 50 and 60, Time elapsed = 40 seconds

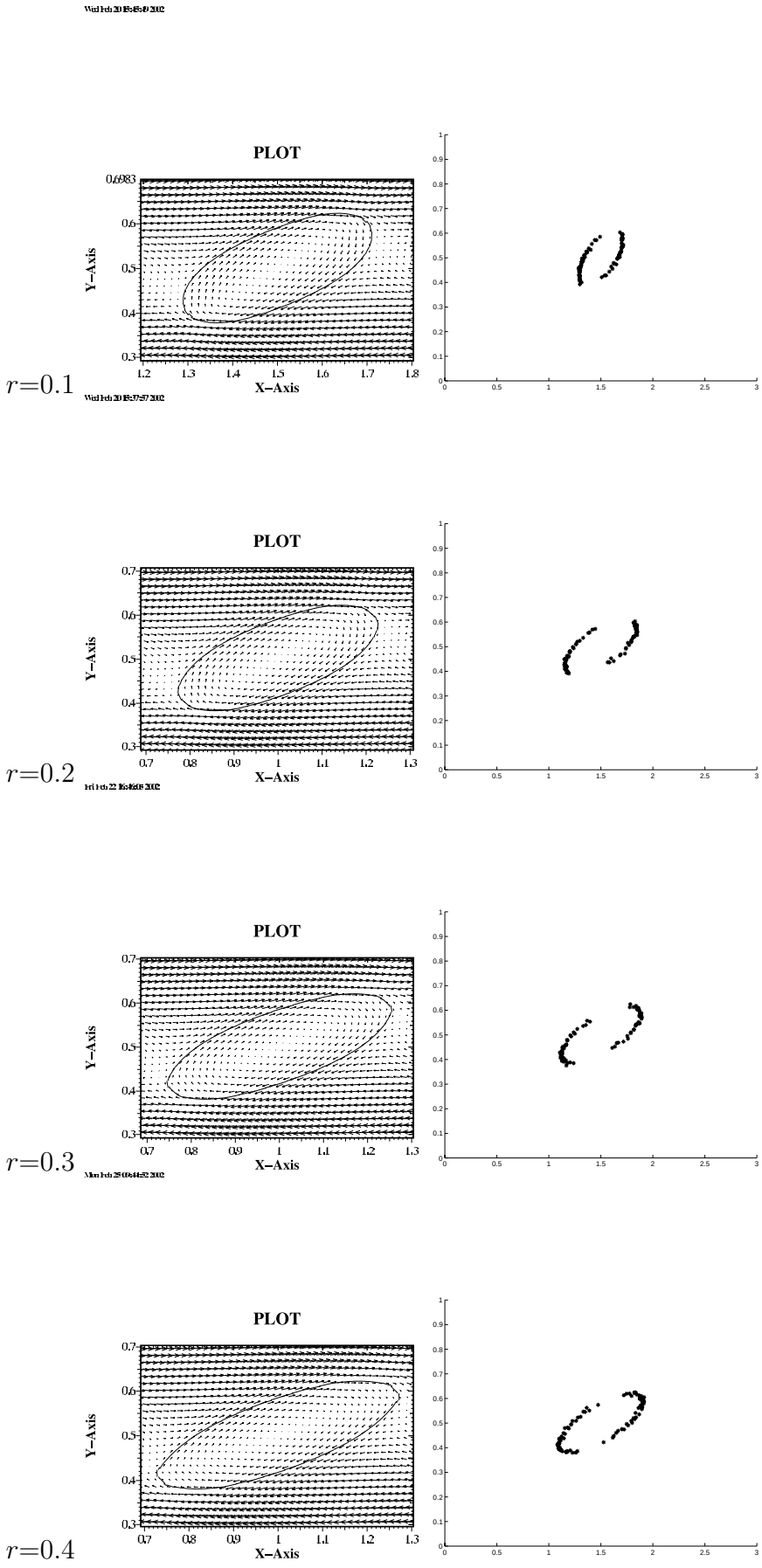

Figure 3.9: Comparison of stable drop configuration under different levels of reduction with surfactant location, Re=1; directly relates to Table 3.3

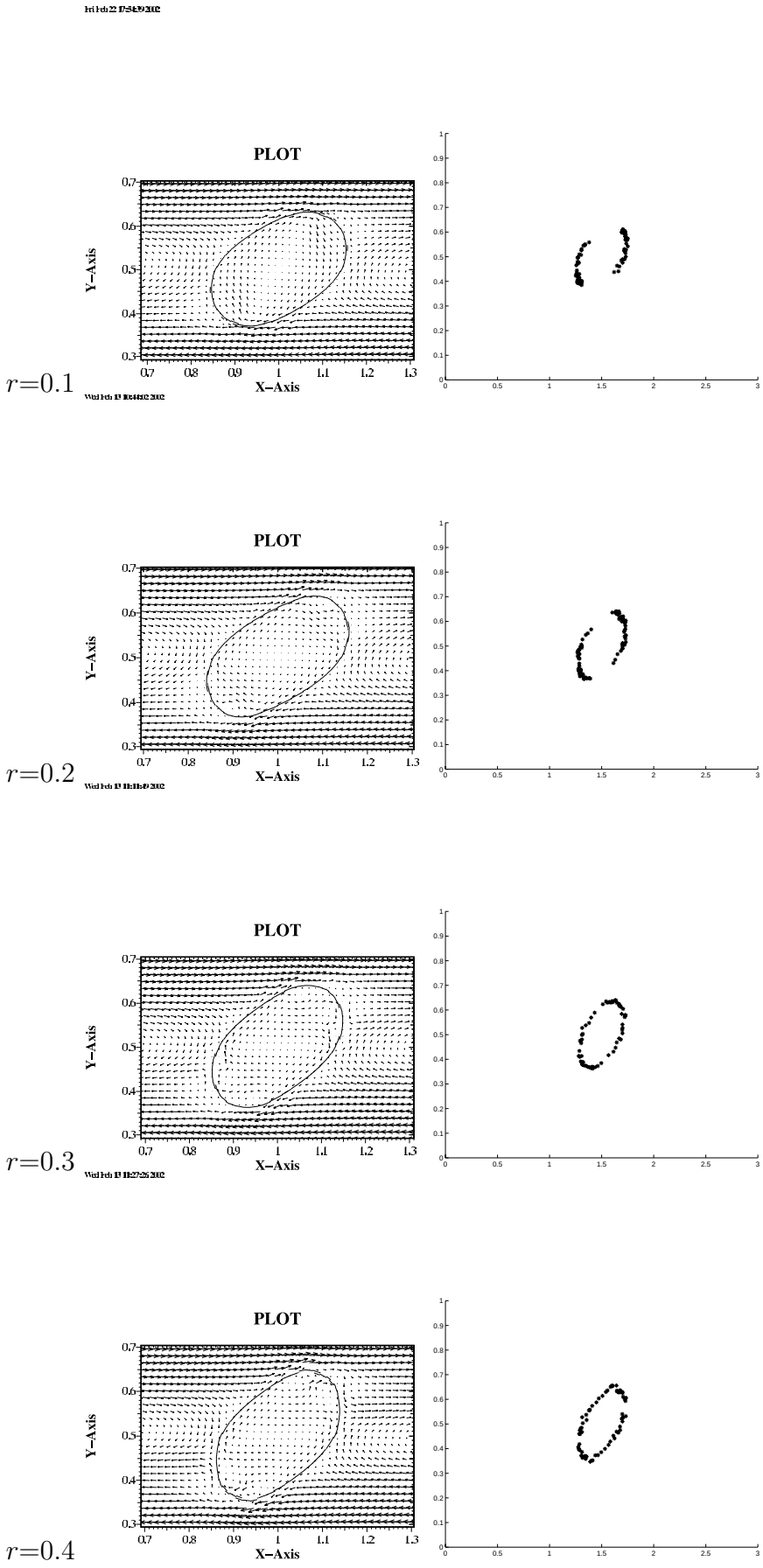

Figure 3.10: Comparison of stable drop configuration under different levels of reduction with surfactant location, Re=60; directly relates to Table 3.3

3.3 Unstable drop evolution

When a stable steady state solution is unavailable, drops become unstable. This means the drops break apart into a collection of daughter drops. The mode of break up may vary depending on the viscosity and density ratios of the system, but for the case of viscosity ratio and density ratio equal to 1, as we have examined in the stable drop evolution, we expect elongation, followed by necking, ending with break up into daughter drops. A similar case with no surfactant is given in [1].

3.3.1 Results

The addition of surfactant speeds the transition to break-up in terms of capillary number; one expects drops of equal Reynolds number coated with surfactant to break at a lower capillary number. Figure 3.11 compares such a break up event at Re=10 at r=0 and r=0.1. In this particular case, break-up occurs at Ca=0.14 (Ca_e=0.155) with surfactant; break-up occurs at Ca=0.15 without surfactant.

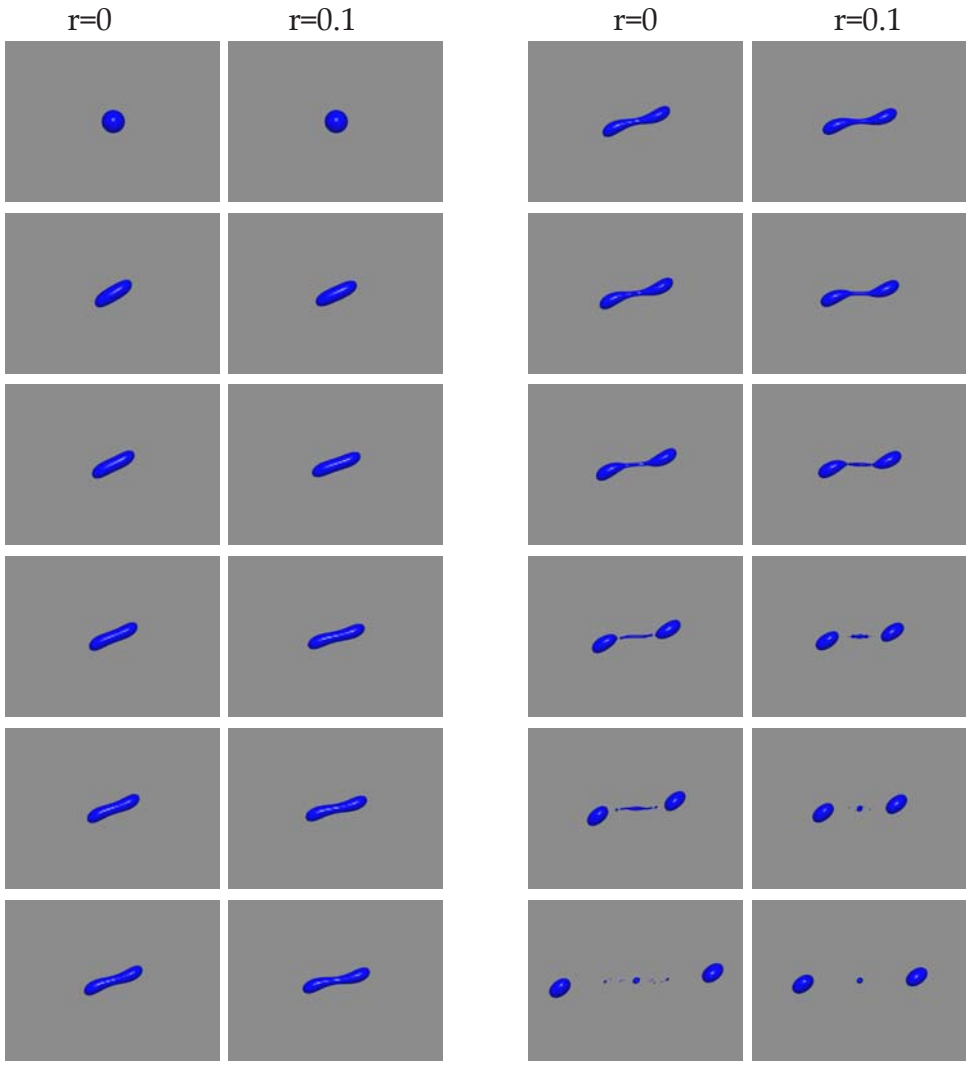

Figure 3.11: Comparing drop breakup with and without surfactant at Re=10. Left columns: Re=10, Ca=0.15, r=0; Right columns: Re=10, Ca=0.14, Ca_e=0.155 Equivalent time progression top to bottom through both columns. t=0, 5, 10, 15, 17, 19, 21, 22, 23, 24, 25, 30 seconds.

The location of surfactant through elongation explains why the drop breaks at a lower capillary number. Initially, the surfactant migrates to the end caps of the drop (just like in the stable case). As the drop begins to neck, the surfactant moves to coat the neck area, thus reducing surface tension in that area and causing break to occur sooner. See Figure 3.12.

If we examine the vector velocity plots of the break up sequence, offsetting the time of breakup to more visually match similar events as in Figure 3.13, we see subtle differences in the break up mode between a case with and without surfactant. When no surfactant is present, just as when the drops went to a stable configuration, the elongated drops are more

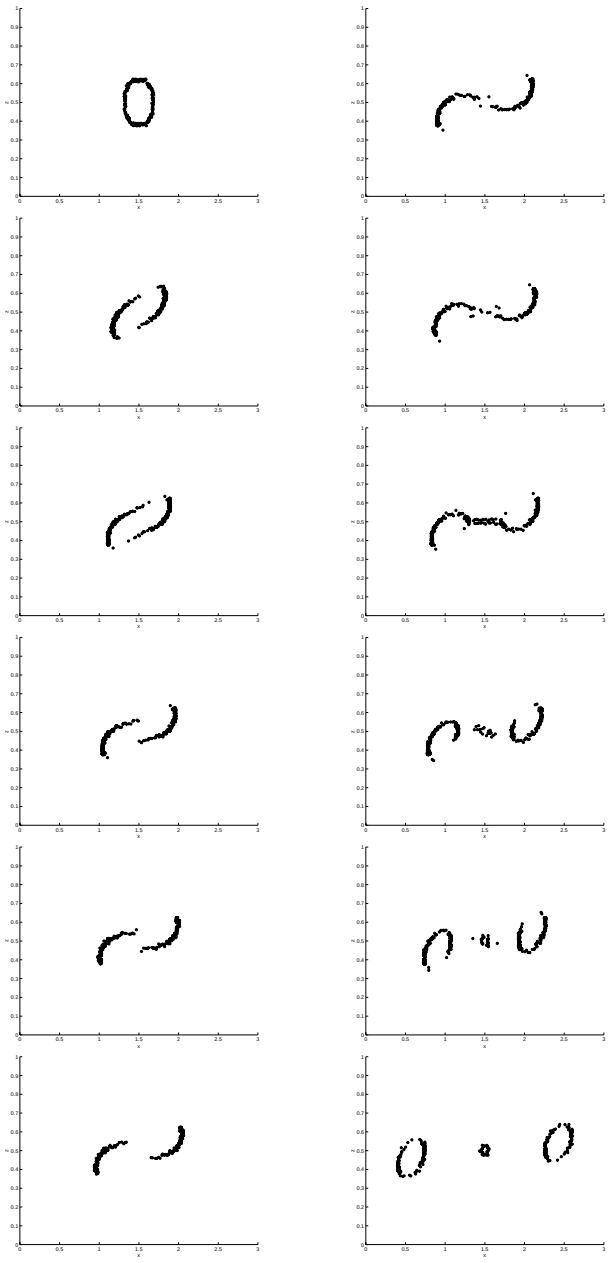

Figure 3.12: Surfactant Migration over time in drop break up. Re=10, Ca=0.14, r=0.1, Top to bottom, Time = 0, 5, 10, 15, 17, 19, 21, 22, 23, 24, 25, 30 seconds

highly inclined with the flow. Also, we can see that the neck area before break up is longer without surfactant. Surface tension in this area would be higher with no surfactant present stabilizing the neck for an instant longer. Once separation is imminent, we can see that neck recoil is less stable in the case without surfactant evident by the multitude of satellite drops created during this process. Surfactant tends to form a 'protective' coating around the recoiling neck resulting in a single satellite drop rather than several smaller satellites.

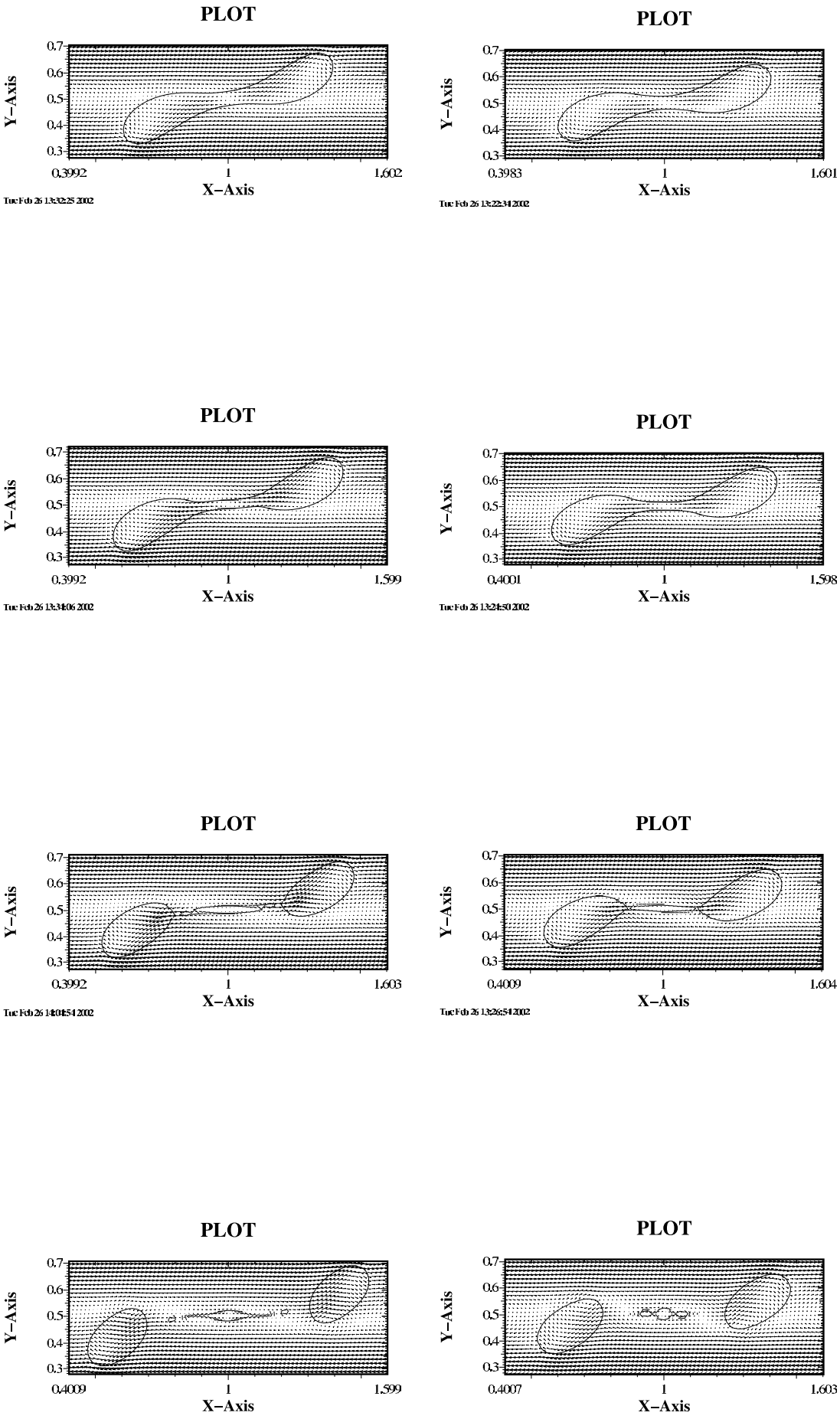

Figure 3.13: Vector velocity plots of break-up area sequence for Re=10; Left: Ca=0.15, r=0; Right: Ca=0.14, Ca_e=0.155, r=0.1; Time (left, top to bottom)= 23, 24, 25, 26 seconds; Time (right, top to bottom) = 22 ,23, 24, 25 seconds. Directly correlates to Figure 3.11.

If we compare drop break-up at higher Re values, we see that surfactant retards breakup. See Figure 3.14. At this Re level, the viscous forces have become so low that inertial forces drive the breakup. The surfactant provides a protective layer against this effect by disrupting the flow near the drop-matrix interface. The general trend of surfactant reducing the angle of inclination of the breakup event remains unchanged. This can further be related to Marangoni forces. Where the surfactant accumulates next to areas of no surfactant, Marangoni stress is elevated. We know from Figure 3.12 that surfactant tends to totally encapsulate a neck through elongation. Marangoni stresses are then concentrated on the bulbuous portions of the drop, lowering the angle of inclination and reducing the tensile force at work in the neck area. By coupling the phenomenon of flow disruption around the neck with a lesser tensile force, the drops break more slowly. Furthermore, "surfactant gradients augment the formation of bulbuous ends and increase the rate of thinning" [52] in the neck region.

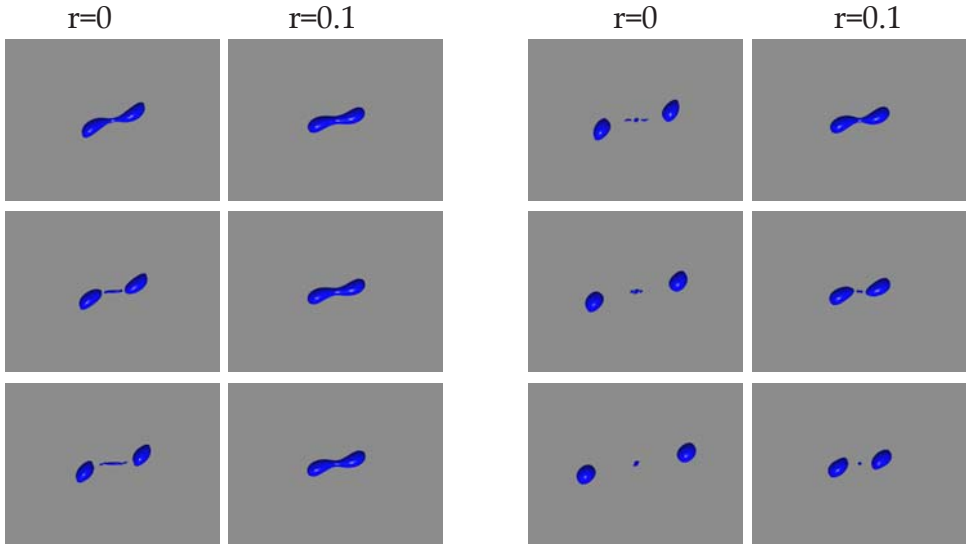

Figure 3.14: Re=50, Ca=0.060, $Ca_{e,r=0.1}$ = 0.066; Comparing drop break up with (right) and without (left) surfactant. Equivalent time progression top to bottom through both columns. t=20, 21, 22, 23, 24, 25 seconds.

To reiterate, on the whole, drop breakup with surfactant at a reduction level of 0.1 results in the breakup mode we expected for this study. The drops elongate, neck and break into symmetric daughter drops. Figure 3.15 represents the full spectrum of Re evaluated in this study at r=0.1.

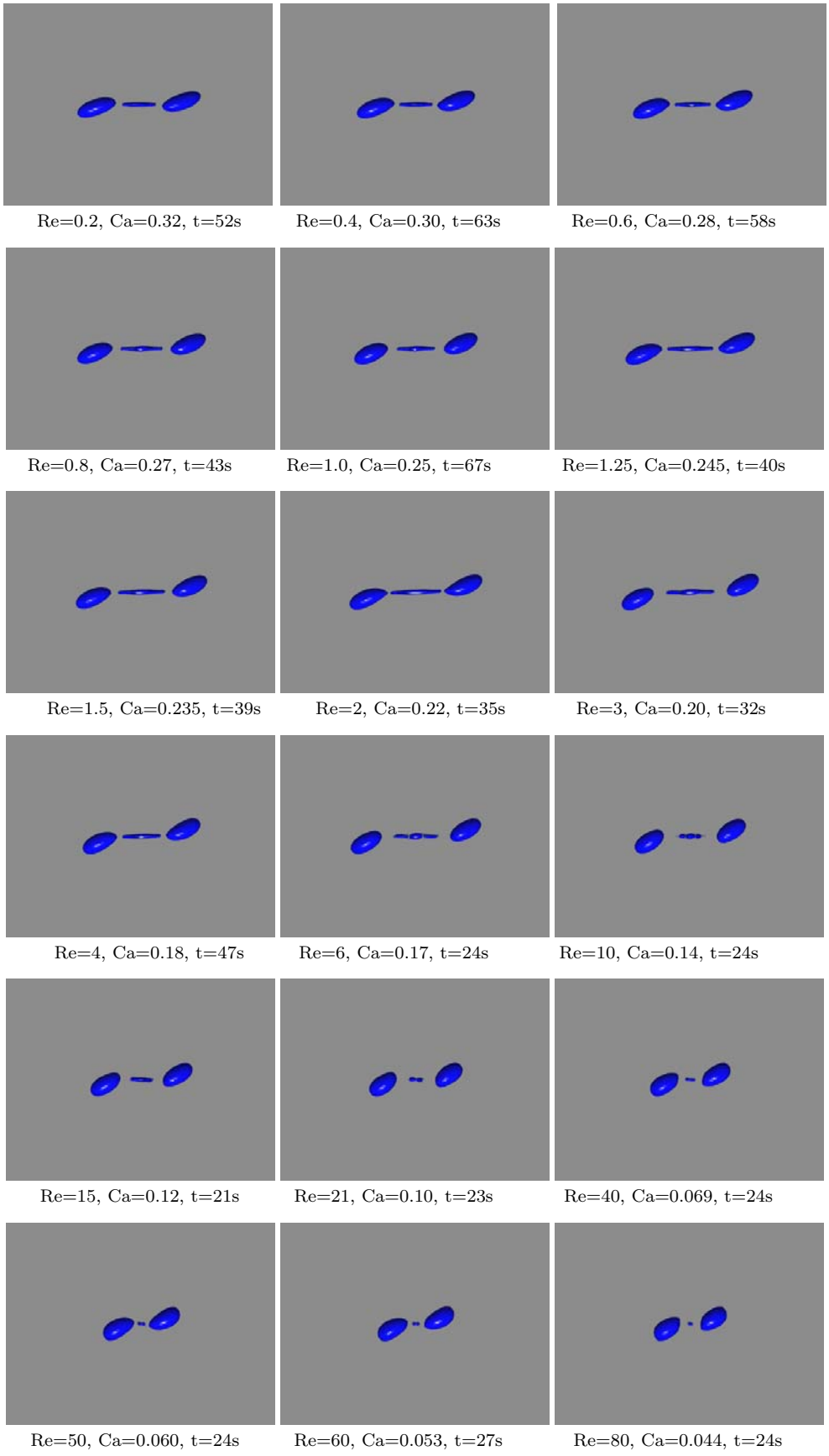

Figure 3.15: Breakup spectrum across study, $0.2 \leqslant \mathrm{Re} \leqslant 80$

3.3.2 Higher levels of reduction

At higher levels of reduction, there is little difference in the physical nature of break-up at similar Re. There is, however, a significant difference in time to break-up as exhibited in Figure 3.16 and Table 3.4. In this depiction, we have essentially matched Ca_e for different levels of reduction at Re=1. At r=0.1, breakup occurs at 67 seconds; at r=0.2, breakup occurs at 57 seconds; at r=0.3, breakup occurs at 40 seconds. The trend is as reduction is increased, time to breakup is decreased. A similar trend emerges for limited Re tested.

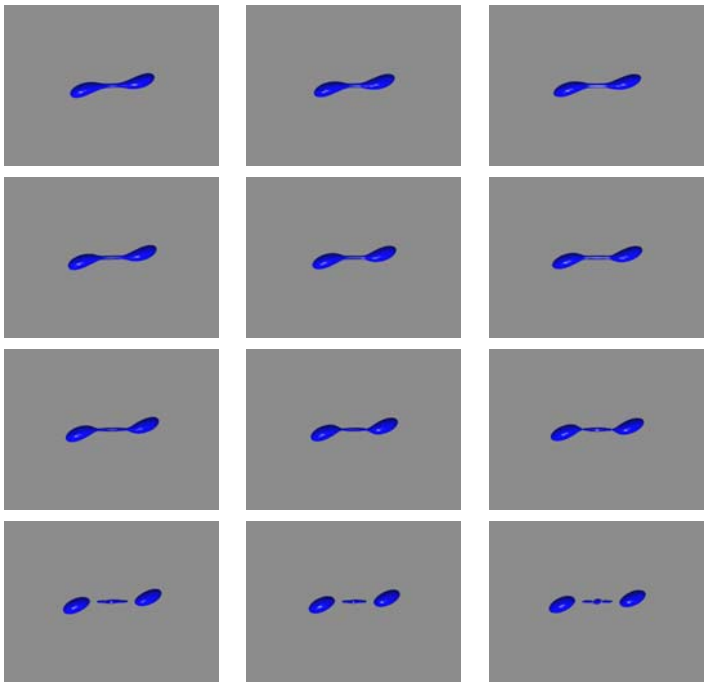

Figure 3.16: Re=1, Column 1: Ca=0.25, Ca_e=0.277, r=0.1, Time = 64, 65, 66, 67 seconds; Column 2: Ca=0.22, Ca_e=0.275, r=0.2, Time = 54, 55, 56, 57 seconds; Column 3: Ca=0.19, Ca_e=0.271, r=0.3, Time = 37, 38, 39, 40 seconds;

Re	Ca	Ca_e	r	Time to breakup (sec)
1	0.28	0.280	0	
	0.25	0.277	0.1	67
	0.22	0.275	0.2	57
	0.19	0.271	0.3	40
50	0.062	0.062	0	30
	0.060	0.066	0.1	28
	0.048	0.060	0.2	26
	0.037	0.052	0.3	23
60	0.054	0.054	0	29
	0.053	0.058	0.1	27
	0.042	0.053	0.2	26
	0.032	0.045	0.3	22

Table 3.4: Time to breakup under different levels of reduction, Re=1, 50 and 60.

Chapter 4

Critical Curves for Small Addition of Surfactant

4.1 Effects of reduction

The primary parameter in high viscosity flow is capillary number (Ca), a measure of the viscous force causing deformation relative to interfacial tension force which keeps a drop together. Recall Equation 2.24. Also recall that when surfactant is added to a system, one must consider an effective capillary number (Ca_e), Equation 2.25, to account for the change in surface tension as it relates to reduction factor, r.

As Reynolds number increases, Reynolds stress is balanced by capillary stress. One expects the inclusion of surfactant to reduce the capillary stress necessary to balance the Reynolds stress. This is generally illustrated in the numerical results of Figure 4.1. Capillary number values below those represented in the figure result in stable drops; larger values result in unstable drops that will break up.

The points at $r = 0$ represented in this figure are the result of a full simulation of the initial value problem, together with the Navier Stokes equation and the continuous surface force formulation with the code SURFER++ [22]. The points at $r = 0.1$ are likewise the result of a full similuation of the initial value problem, together with the Navier Stokes equation and the continuous surface stress formulation with no smoothing as conducted with the code SURFER++. The computations at $r = 0$ were performed in the computational domain 1 x $\frac{1}{2}$ x 1, with a 64 x 32 x 64 mesh, and initial drop radius $a = 0.125$, timesteps $10^{-3}\dot{\gamma}^{-1}$. The computations at $r = 0.1$ were performed in the computational domains described in Chapter 3, but with similar radius and timestep requirements.

At $r = 0.1$, for Reynolds numbers greater than 60, the capillary stress necessary to balance the Reynolds stress becomes larger, crossing the threshhold values seen for $r = 0$. See Figure 4.2.

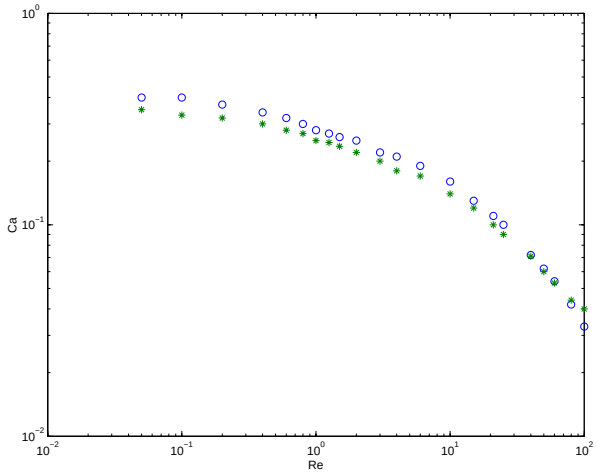

Figure 4.1: Re vs. Ca, viscosity ratio=1, equal densities, o r=0, * r=0.1

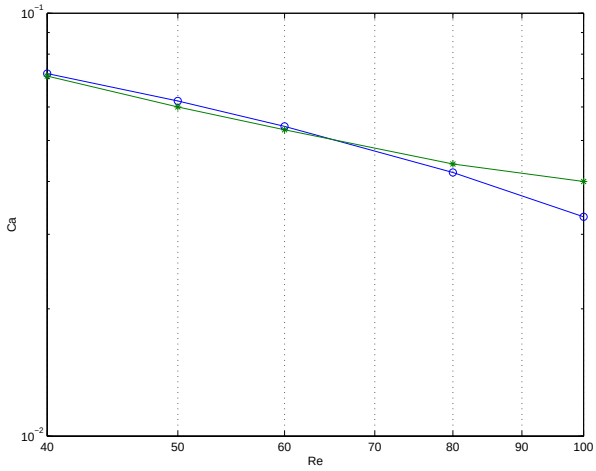

Figure 4.2: Re vs. Ca, viscosity ratio=1, equal densities, o r=0, * r=0.1

The crossover point indicates a balance between viscous and inertial stresses. Examining velocity vector plots of stable drops to the immediate left and right of the crossover point does not in itself clarify a distinct physical change in this area. In fact, Figures 4.3 and 4.4 look extremely similar. The intensity of the vortical motion inside the drop is more evident in the cases without surfactant, but there are similar, though less intense, vortices in the drops coated with surfactant. The physical geometry is different between the two cases; the non-surfactant case exhibits heavier tip pointing, but this is expected as the angle of inclination increases against the base flow. The generally round tips seen in the cases with surfactant are likewise expected as the surfactant lowers surface tension in these areas as noted in Figure 3.3 from Chapter 3.

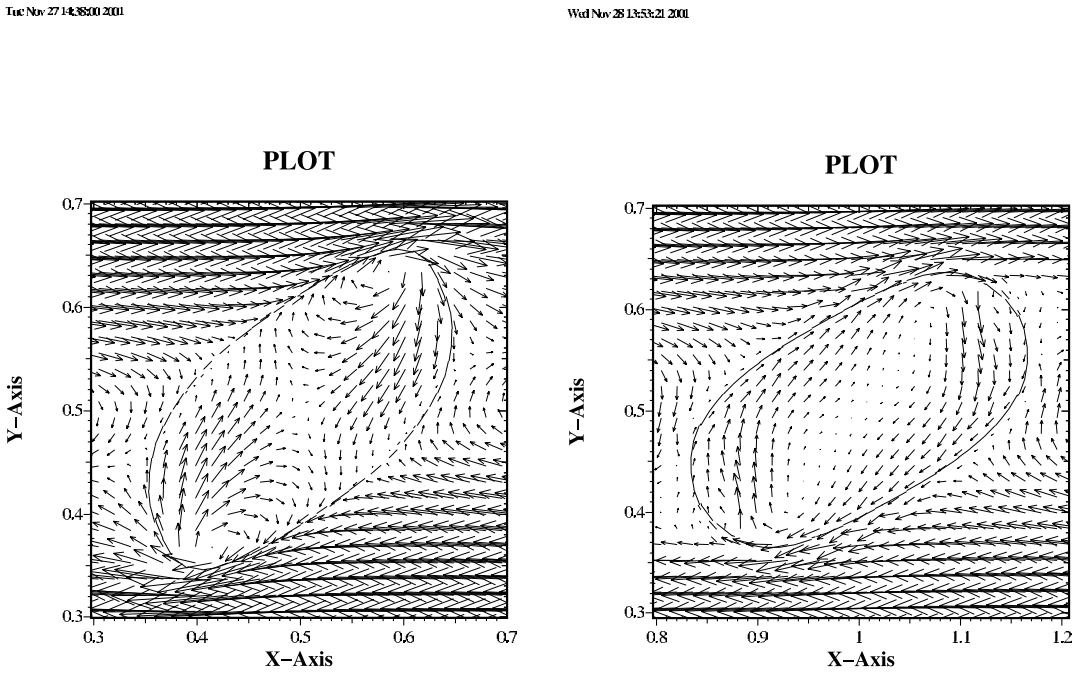

Figure 4.3: Left of Crossover, Velocity vector plots, just below criticality, Re=60, left: r=0, right: r=0.1

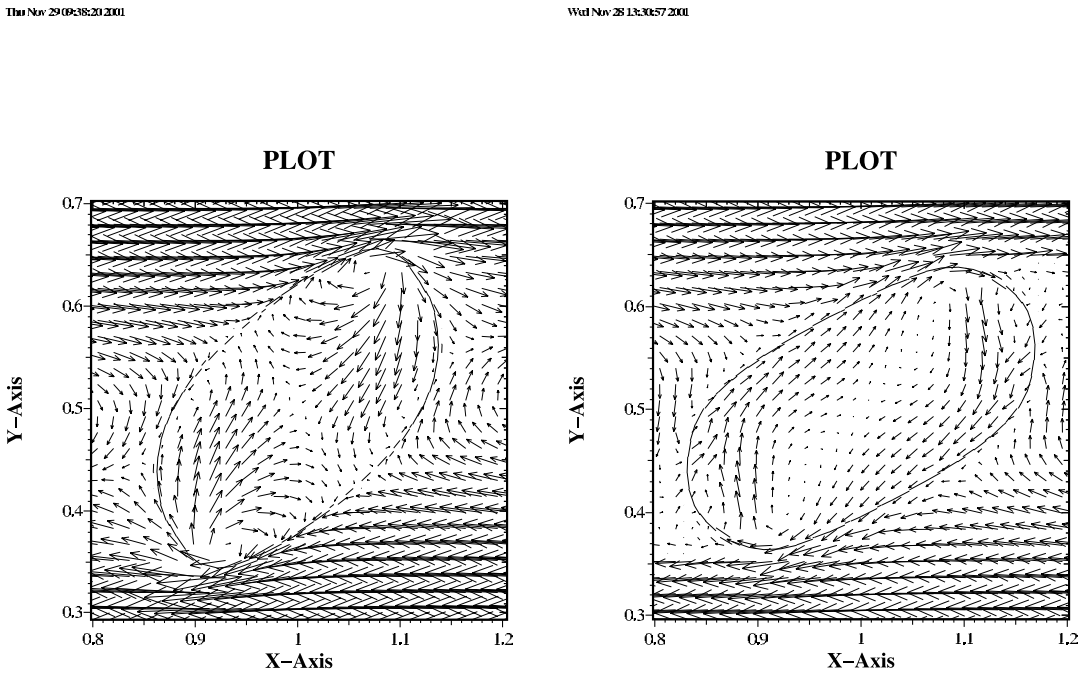

Figure 4.4: Right of Crossover, Velocity vector plots, just below criticality, Re=80, left: r=0, right: r=0.1

Ideally, if we look specifically at effective capillary number for the case of reduction = 0.1, we would see the stability curves at r=0 and r=0.1 completely overlap. Instead, we see the r=0.1 curve go above the r=0 curve. Here we notice that the crossover actually occurs at Re=40. See Figure 4.6 If we examine velocity vector plots of stable drops to the left and right of this new crossover point, there is one distinct physical difference. To the left of the crossover, at Re=10 (Figure 4.7) the drop with surfactant has only one center of circulation. Beyond the crossover point at Re=60 (Figure 4.8), we see the full formation of two centers of circulation. The development of secondary centers of circulation indicates stronger inertial forces at work. The surfactant, however, reduces interfacial tension enough so that we see a flattening of the drop end caps, keeping the angle of inclination low, retarding breakup.

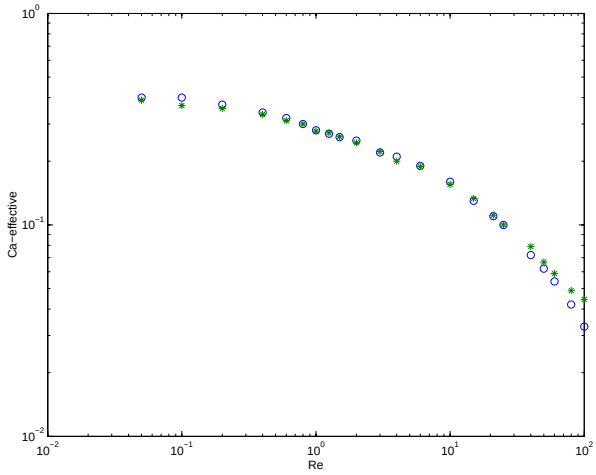

Figure 4.5: Re vs. Ca_e, viscosity ratio=1, equal densities, o r=0, * r=0.1

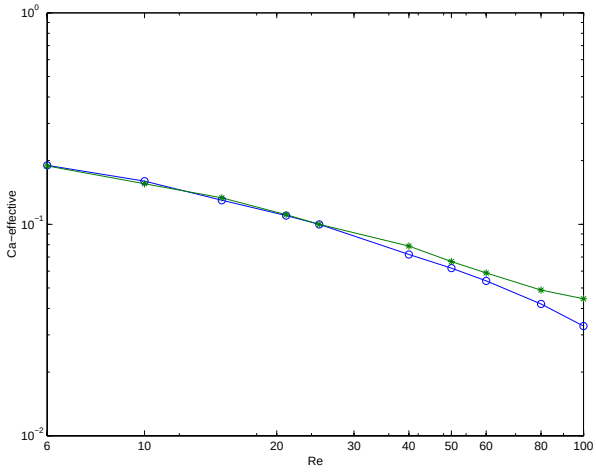

Figure 4.6: Re vs Ca_e, viscosity ratio=1, equal densities, o r=0, * r=0.1

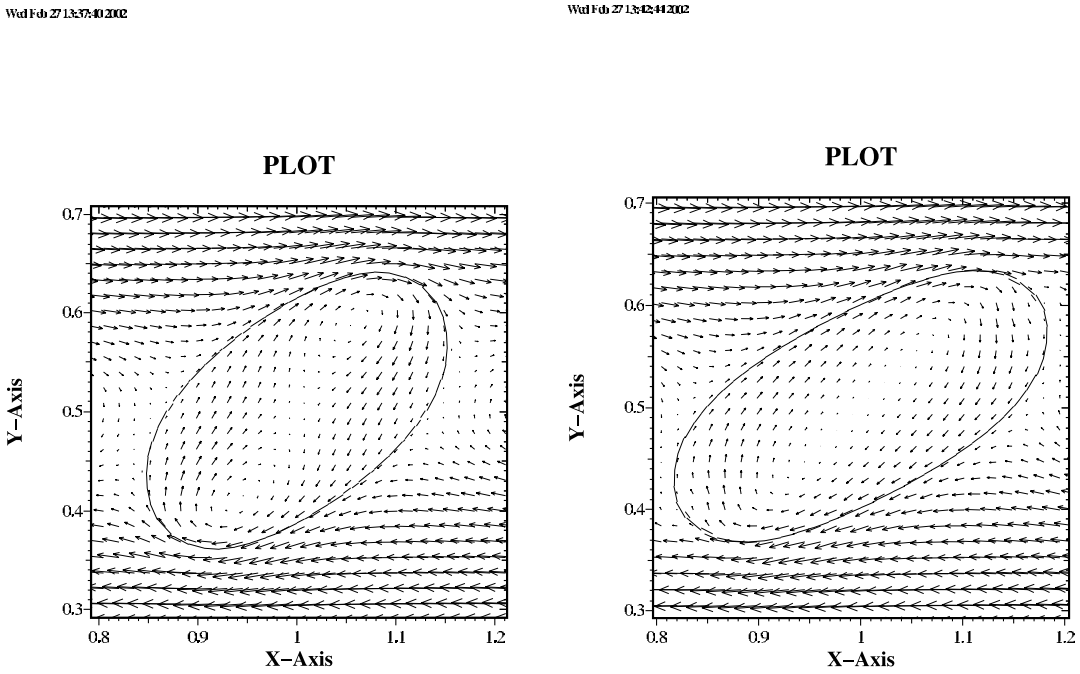

Figure 4.7: Left of Effective Capillary Number Crossover, Velocity vector plots, just below criticality, Re=10, left: r=0, right: r=0.1

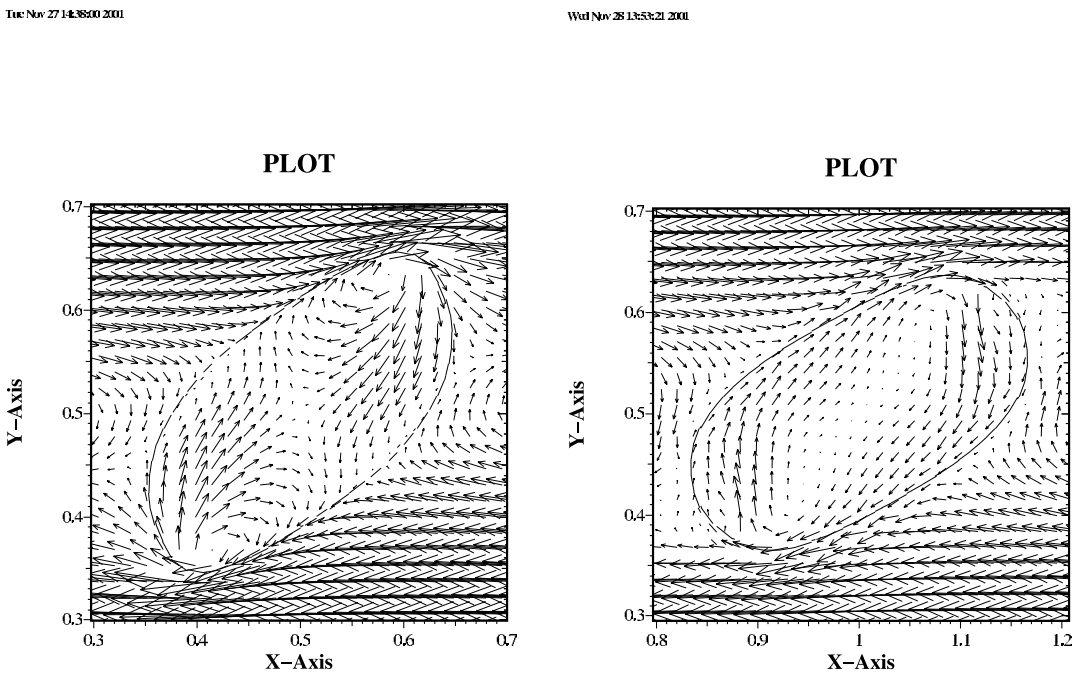

Figure 4.8: Right of Effective Capillary Number Crossover, Velocity vector plots, just below criticality, Re=60, left: r=0, right: r=0.1

4.2 Higher reduction

As surface tension is reduced, numerical simulation verifies the theoretical prediction that the transition between stable and unstable drops becomes evident at lower capillary number. See Figure 4.2.

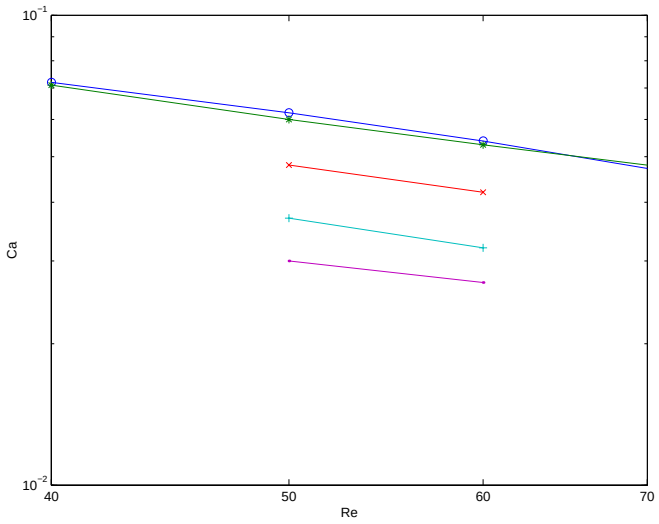

Figure 4.9: Re vs. Ca, viscosity ratio=1, equal densities, o r=0, * r=0.1, x r=0.2, + r=0.3, r=0.4

Particular geometry differences resulting from an increase in reduction including a change in surfactant distribution is given in Sections 3.2.2 (stable drop evolution) and 3.3.2 (unstable drop evolution).

Chapter 5

Effect of Surfactant on Daughter Drops

As drops breakup they evolve into daughter drops. First daughters are those components that break off first. In these studies, first daughters refer to the largest remnants of breakup. There are always two such daughters in the work presented here. Data given throughout this section are related to a single first daughter as the two are physically symmetric. Necks refer to the center extensional area. They usually recoil into a single small satellite or several very small satellites. These are not included in the daughter drop analysis, but are handled separately and in a more qualitative way.

5.1 Necking

Generally speaking, the addition of surfactant reduces neck length at breakup. Recall Figure 3.11. When reduction is held constant, the trend at breakup is as Re increases, neck length decreases. Essentially, at higher viscosity, we expect to see longer necks. The simulations performed for this study do not result in specific neck length measurements but a quick visual inspection of velocity vector plots one second before breakup verify this statement. See Figures 5.1 and 5.2. Similarly, Table 5.1 iterates the number of mesh cells the neck spans for each case.

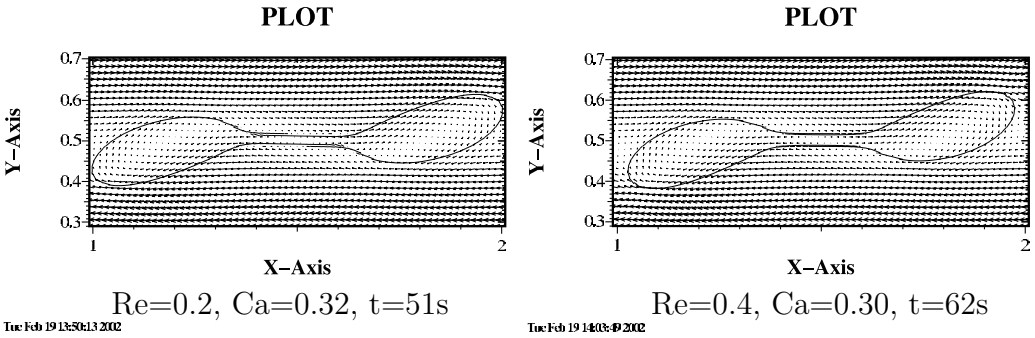

Re=0.2, Ca=0.32, t=51s

Re=0.4, Ca=0.30, t=62s

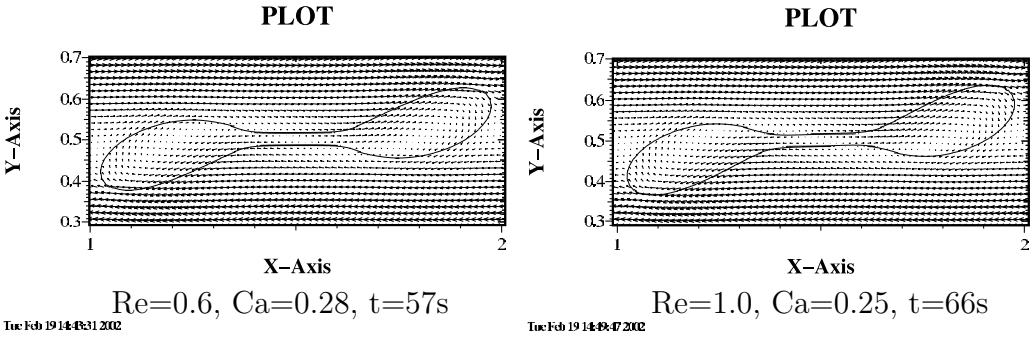

Re=0.6, Ca=0.28, t=57s

Re=1.0, Ca=0.25, t=66s

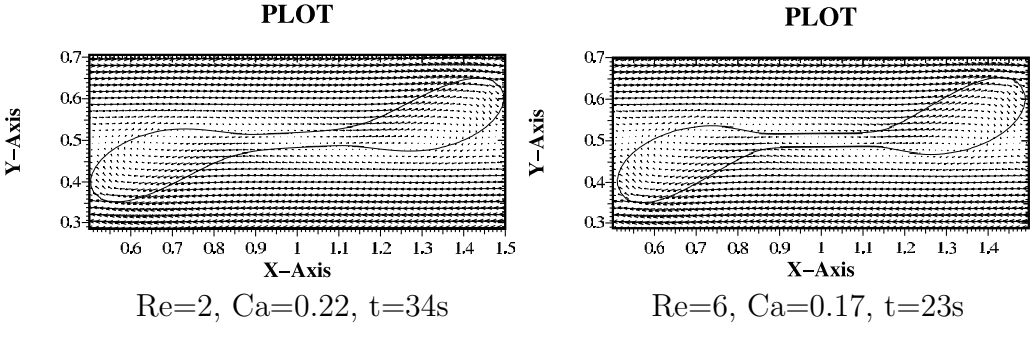

Re=2, Ca=0.22, t=34s

Re=6, Ca=0.17, t=23s

Figure 5.1: Necking 1 second before breakup, r=0.1, $0.2 \leqslant \mathrm{Re} \leqslant 6$

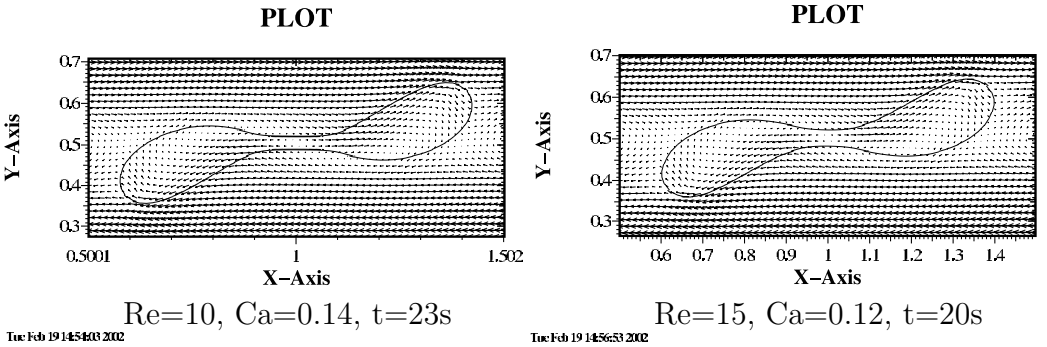

Re=10, Ca=0.14, t=23s Re=15, Ca=0.12, t=20s

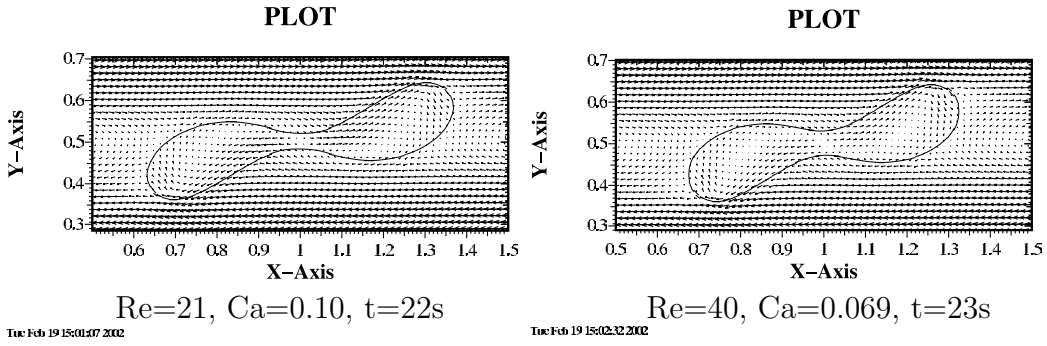

Re=21, Ca=0.10, t=22s Re=40, Ca=0.069, t=23s

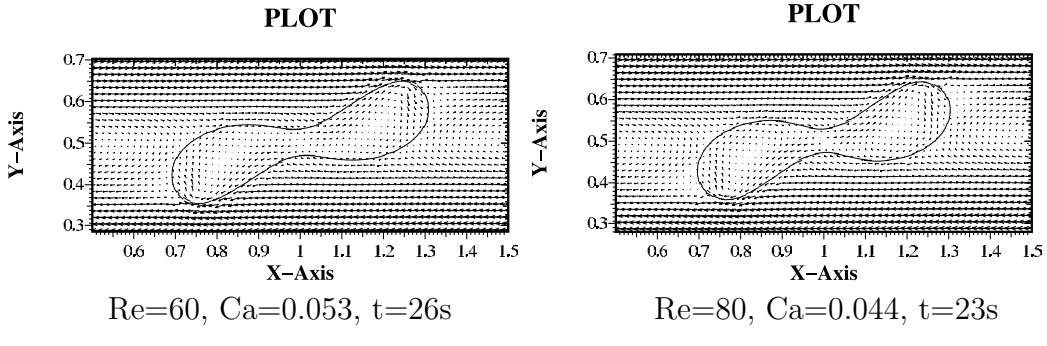

Re=60, Ca=0.053, t=26s Re=80, Ca=0.044, t=23s

Figure 5.2: Necking 1 second before breakup, r=0.1, $10 \leqslant \mathrm{Re} \leqslant 80$

Re	Ca	Ca_e	Neck Length
			(spanned mesh cells)
0.2	0.32	0.355	13
0.4	0.30	0.333	13
0.6	0.28	0.311	12.5
1.0	0.25	0.277	12
2.0	0.22	0.244	11
6.0	0.17	0.188	11
10.0	0.14	0.155	9
15.0	0.12	0.133	6
21.0	0.10	0.111	4
40.0	0.069	0.0766	3
50.0	0.060	0.0666	3
60.0	0.053	0.0588	3
80.0	0.044	0.0488	2

Table 5.1: Neck Lengths 1 second before break across Re, r=0.1

5.2 Daughter drop critical curve

Daughter drops pinch off from an elongated neck as a natural mechanism to reduce surface area. This is an effect caused by the chaotic need to reduce surface tension thereby reducing the energy of a system. Once daughter drops are created from a breakup event, the daughter drops act like individual droplets themselves. Figure 5.3 represents the Reynolds and capillary number relationship between mother and daughter drops for the critical capillary number associated with the mother drop for both r=0 and r=0.1.

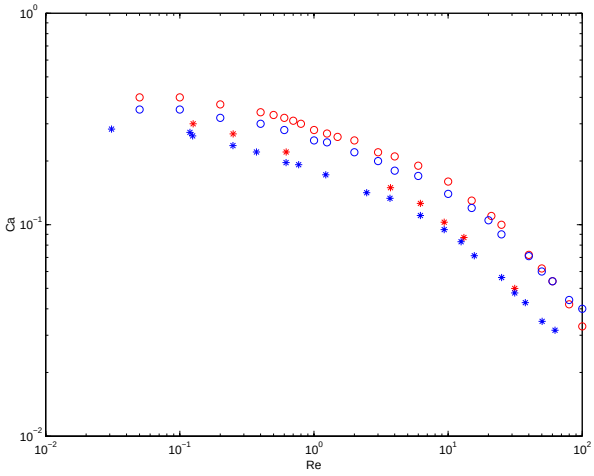

Figure 5.3: Daughter drop critical curves. Red: r=0, Blue: r=0.1, o: mother, *: daughter

If we instead look at Ca_e for the daughter drops, just as for the mother drops, we expect the r=0.1 data to overlay the r=0 data. See Figure 5.4.

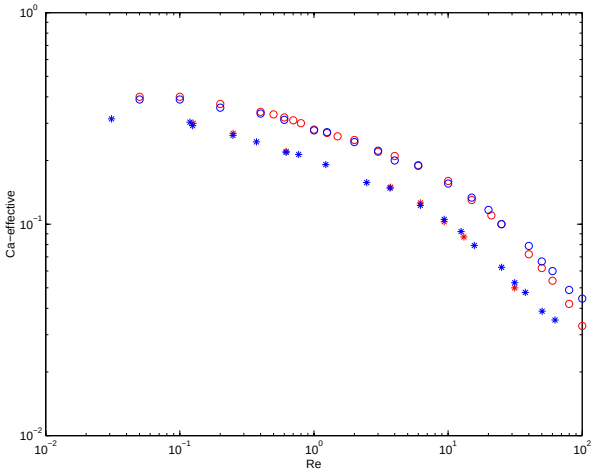

Figure 5.4: Daughter drop critical curves in terms of Ca_e. Red: r=0, Blue: r=0.1, o: mother, *: daughter

5.3 Daughter drop volumes

Once the first daughter drops are pinched off and behaving as independent drops, a question arises as to their physical construct. Specifically, we are interested in their volume. It is of notice that despite Re, the first daughter drops in this study all have close to the same volume, roughly 4 x 10^{-3} units. See Table 5.2. This is also independent of the inclusion of surfactant. At best a difference of less than 2% arises.

r = 0					r = 0.1				
Mother		Daughter			Mother		Daughter		
Re	Ca	Re	Ca	Volume	Re	Ca	Re	Ca	Volume
				(x10^{-3})					(x10^{-3})
0.05	0.40				0.05	0.36	0.0309	0.2831	3.97
0.20	0.37	0.1255	0.3000	4.06	0.20	0.32	0.1245	0.2630	4.01
0.40	0.34	0.2498	0.2687	4.03	0.40	0.30	0.2488	0.2366	4.01
0.60	0.32				0.60	0.28	0.3722	0.2205	3.99
0.80	0.30				0.80	0.27			
1.0	0.28	0.6206	0.2206	3.99	1.0	0.25	0.6189	0.1933	3.98
1.25	0.27				1.25	0.245	0.7689	0.1922	3.94
1.50	0.26				1.50	0.235	0.9220	0.1842	3.94
2.0	0.25				2.0	0.22	1.2246	0.1722	3.91
3.0	0.22				3.0	0.20			3.93
4.0	0.21				4.0	0.18	2.4739	0.1416	3.97
6.0	0.19	3.7193	0.1496	3.99	6.0	0.17	3.6886	0.1333	3.94
10.0	0.16	6.2125	0.1261	4.00	10.0	0.14	6.2209	0.1104	4.01
15.0	0.13	9.3626	0.1027	4.03	15.0	0.12	9.3623	0.0948	4.03
21.0	0.11	13.1200	0.0870	4.03	21.0	0.10	13.1609	0.0792	4.05
25.0	0.10				25.0	0.090	15.6862	0.0713	4.06
40.0	0.072				40.0	0.071	25.0908	0.0562	4.06
50.0	0.062	31.3900	0.0499	4.06	50.0	0.060	31.4132	0.0476	4.07
60.0	0.054				60.0	0.054	37.6919	0.0428	4.07
80.0	0.042				80.0	0.044	50.2830	0.0349	4.07
100.0	0.033				100.0	0.040	62.6930	0.0317	4.06

Table 5.2: Daughter drop comparative data: $r = 0$ and $r = 0.1$

Similarly, if we examine the velocity vector profile of a first daughter, we see a singular pattern arise whereby the daughter contains one vortical center across all Re. See Figure 5.5. Of course the amount of elongation within the daughter varies at the different viscosities illustrated, but the general pattern is identical.

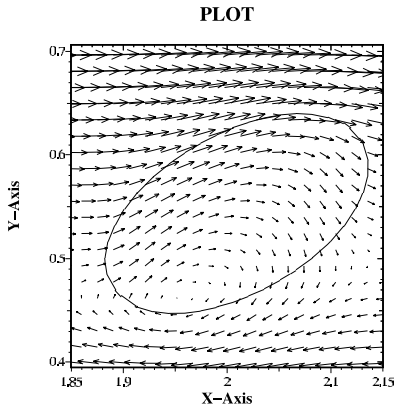

Re=1, Ca_D=0.1933

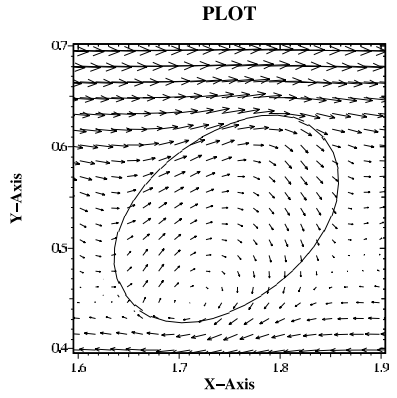

Re=10, Ca_D=0.1104

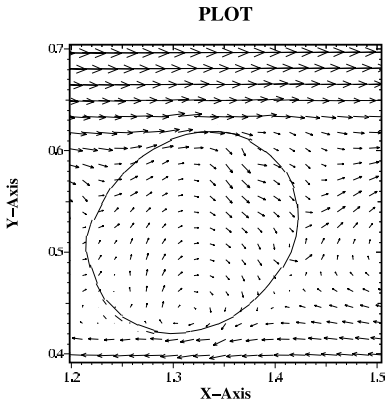

Re=100, Ca_D=0.0317

Figure 5.5: Velocity vector plot of first daughter drops, Re = 1, 10, 100; r=0.1

5.4 A numerical experiment

Renardy and Cristini [49] offer a numerical experiment designed to emulate a spherical drop suspended in a matrix liquid of the same viscosity and density that is then sheared. They indicate that just above the critical capillary number, first daughter drops are roughly 50% of the original volume of the initial drop. They further demonstrate that by varying initial drop size, and relating Reynolds and Capillary number by the relationship

$$\frac{\mathrm{Re}}{Ca^2} = K, \tag{5.1}$$

where

$$K = \frac{\rho\sigma^2}{\mu^3\dot{\gamma}} \tag{5.2}$$

is a constant, that daughter drops will saturate to predictable volumes along these parabolic curves.

Constructing a parabola along the path $\mathrm{Re} = 391 * Ca^2$, which coincides with Figure 1 of [49], similarly illustrates that the addition of surfactant still results in predictable daughter drop data. Figure 5.6 illustrates the parabola in question in the Re-Ca plane together with the critical curves for r=0 and r=0.1. The intersection of the parabola with the curve illustrating r=0.1 occurs at Ca_c, the critical capillary number. The circles along the parabola represent different values for a mother drop. Figure 5.7 illustrates that the daughter drops in the experiment saturate to roughly 49% of the critical volume. This is in contrast to Renardy and Cristini's drops which saturate between 50 and 60%. This indicates that the addition of surfactant results in smaller first daughters as volume of the mother drop is increased.

Figure 5.8 shows how the drops look just after the first daughters pinch away from the neck. Notice how increasing capillary number results in more highly elongated and larger volume necks. First daughters, however, are not geometrically similar. This is also in contrast to Renardy and Crisitini's work as seen in Figure 5.10. Typical surfactant location for the experiment (after break up) is shown in Figure 5.9. By lowering surface tension only in the area where surfactant is shown, the regular and smooth shape expected by a natural distribution of surface tension, does not manifest itself. Instead, we see more irregularly shaped daughter drops. Recall, however, that volumes are predictable.

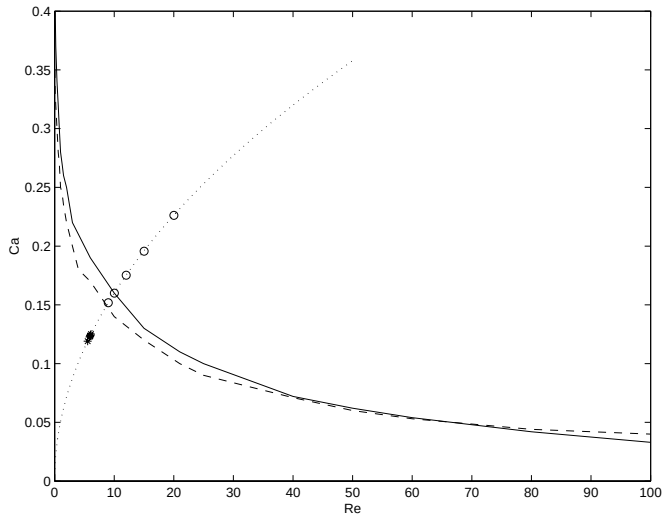

Figure 5.6: Re v. Ca for critical curves at r=0 (solid), r=0.1 (dashed); Re=$391 * Ca^2$, fluid properties and flow strength fixed, radius of mother drop varies; Circles represent mother drops associated with Re=9, Ca=0.1517; Re=10, Ca=0.16; Re=12, Ca=0.1752; Re=15, Ca=0.1959; Re=20, Ca=0.2263; Stars represent daughter drop relationships at break up.

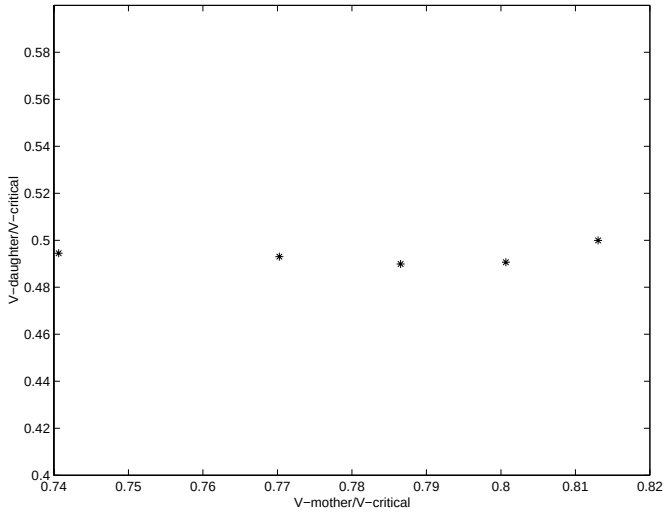

Figure 5.7: Ratio of volumes demonstrates that daughter drops saturate to to roughly 49% of the critical volume.

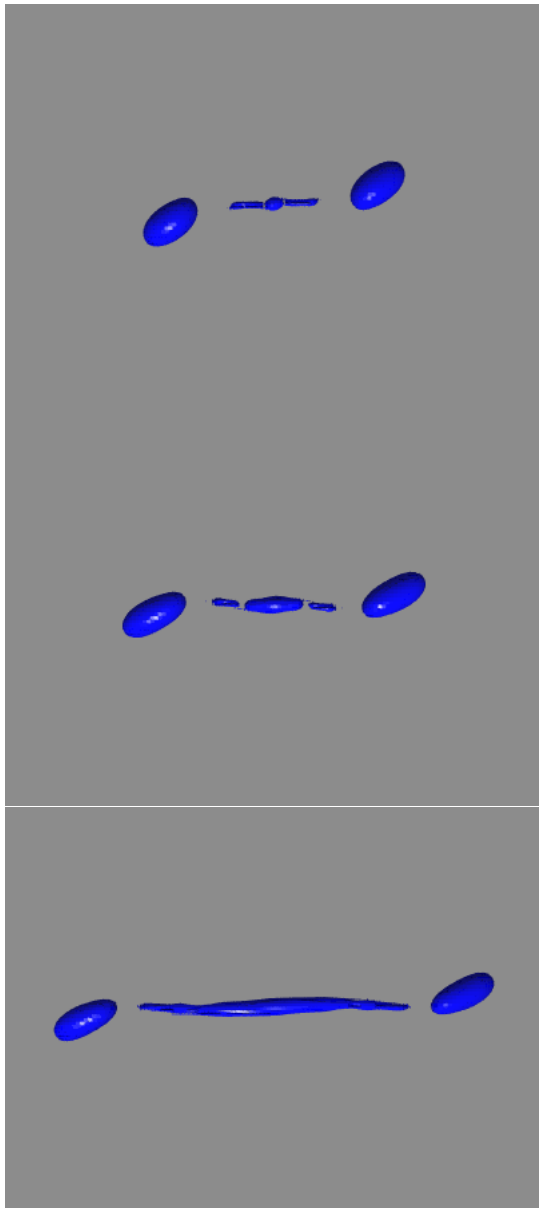

Figure 5.8: Pinch off of daughter drops associated with Figure 5.6 Top to bottom: Re=9, Ca=0.1517, t=Xs; Re=10, Ca=0.16, t=20s; Re=12, Ca=0.1752, t=21s.

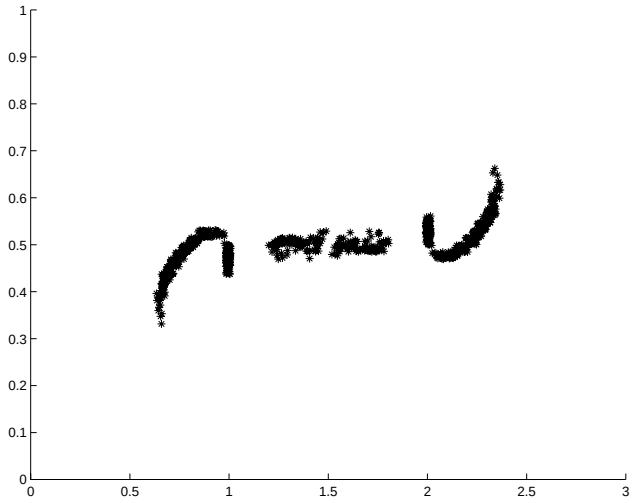

Figure 5.9: Surfactant location for Re=9, Ca=0.1517, t=28s; surfactant stagnates on daughter drops

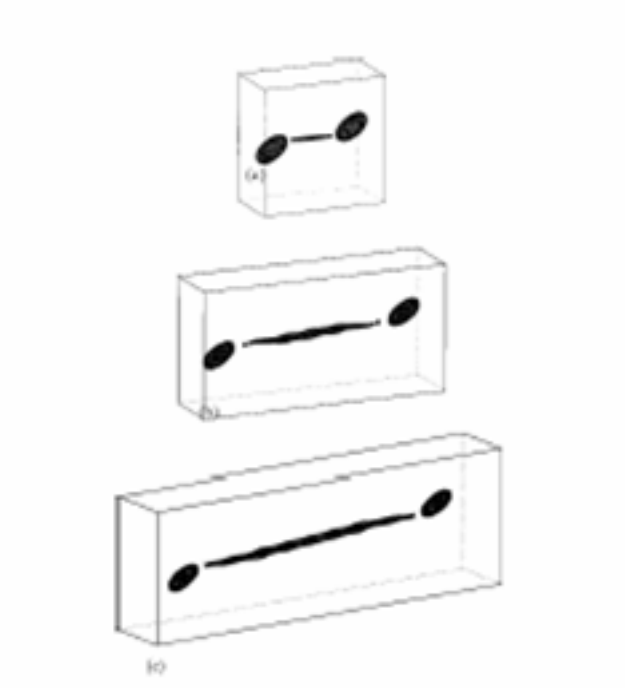

Figure 5.10: FIG. 2. from [49]. Pinch off daughter drops (no surfactant) for (a) Re=10, Ca=0.16, t=19.5s, (b) Re=12, Ca=0.1753s, t=18s, (c) Re=15, Ca=0.196, t=18.6s. We see geometrically similar daughter drops.

5.5 Higher reduction

At higher reduction levels there is little change in the volume associated with the first daughter drops. However, the single vortical motion damps out as reduction increases. At r=0.4, the flow inside the daughter drop is almost aligned with the primary flow. See Table 5.3 and Figure 5.11.

	Re_D	Ca_D	$radius_D$	$Volume_D$
			(x10^{-2})	(x10^{-3})
Re = 1				
$r = 0$	0.6206	0.2206	9.839	3.99
$r = 0.1$	0.6189	0.1933	9.833	3.98
$r = 0.2$	0.6209	0.1733	9.850	4.00
$r = 0.3$	0.6184	0.1494	9.829	3.98
$r = 0.4$				
Re = 50				
$r = 0$	31.3900	0.0499	9.904	4.06
$r = 0.1$	31.4132	0.0476	9.907	4.07
$r = 0.2$	31.3766	0.0380	9.902	4.06
$r = 0.3$				
$r = 0.4$	31.0179	0.0252	9.845	3.99
Re = 60				
$r = 0$				
$r = 0.1$	37.6919	0.0428	9.907	4.07
$r = 0.2$	37.6741	0.0332	9.905	4.07
$r = 0.3$	37.6243	0.0253	9.898	4.06
$r = 0.4$	36.7473	0.0234	9.782	3.92

Table 5.3: Effect of higher reduction on first daughter drops: Re = 1, 50, 60

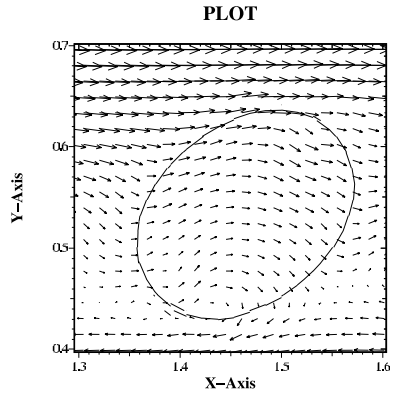

Re=60, Ca_D=0.0428, r=0.1

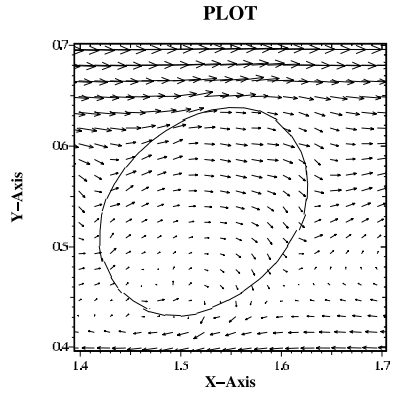

Re=60, Ca_D=0.0332, r=0.2

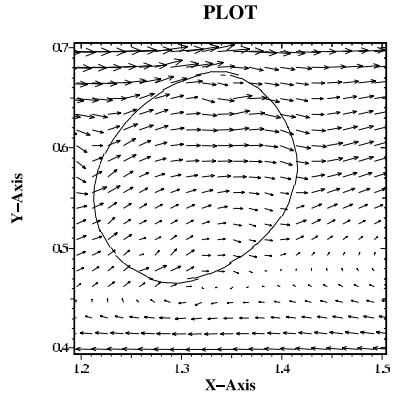

Re=60, Ca_D=0.0253, r=0.3

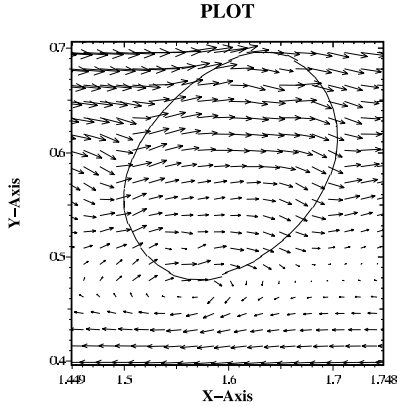

Re=60, Ca_D=0.0234, r=0.4

Figure 5.11: Velocity vector plot of first daughter drops, Re = 60; r=0.1, 0.2, 0.3, 0.4

Chapter 6

Numerical Accuracy

To test numerical accuracy of the data given throughout this work, evaluations were made using a more refined spacial mesh and time step plus expanded box sizes to verify that consistent data were created. Accuracy tests are shown on a breakup sequence to demonstrate the greatest change in interface position.

6.1 Refined spatial mesh

A refined spatial mesh of $\frac{1}{96}$ was evaluated and compared to a similar run using a spatial mesh of $\frac{1}{64}$.

Table 6.1 compares the data generated for a typical breakup sequence. The data are the result of a full simulation of the initial value problem, together with the Navier Stokes equation and the continuous surface stress with no smoothing formulation incorporating surfactant with the code SURFER++. The computations were performed in the computational domain 2 x $\frac{1}{2}$ x 1, with an initial drop radius $a = 0.125$, and timesteps $10^{-3}\dot{\gamma}^{-1}$.

Spatial Mesh Size	Re_D	Ca_D	$radius_D$	$Volume_D$	Time to Break
			(x10^{-2})	(x10^{-3})	(seconds)
$\frac{1}{64}$	6.2208	0.1104	9.859	4.01	24
$\frac{1}{96}$	6.2269	0.1104	9.863	4.02	24
—% Error—	0.09	0.04	0.04	0.14	0

Table 6.1: Refined Spatial Mesh: Error Measurment for Re=10, Ca=0.14, Ca_e=0.155, r=0.1, Breakup sequence

Although numerically similar, there are some visual differences in the simulation output primarily in the neck region. As the formation of these minor satellites is not the emphasis of this work, a $\frac{1}{64}$ spatial mesh is acceptable. See Figure 6.1.

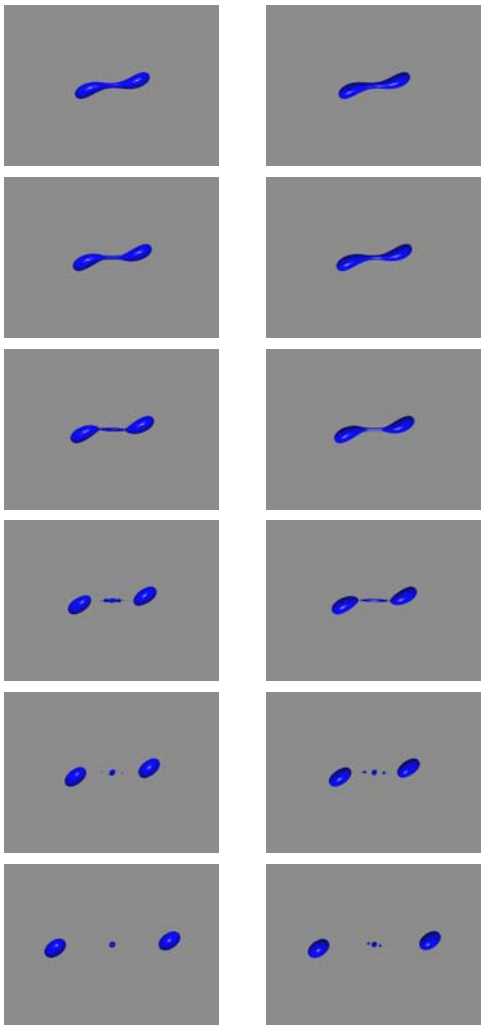

Figure 6.1: Refined Spatial Mesh: Visual Breakup Sequence for Re=10, Ca=0.14, Ca_e=0.155, r=0.1, Left: $\frac{1}{64}$ mesh, Right: $\frac{1}{96}$ mesh, Top to Bottom: Time = 21, 22, 23, 24, 25, 30 seconds

6.2 Refined time steps

A refined time step of $10^{-4}\dot{\gamma}^{-1}$ was evaluated and compared to a similar run using a time step of $10^{-3}\dot{\gamma}^{-1}$.

Table 6.2 compares the data generated for a typical breakup sequence. The data are the result of a full simulation of the initial value problem, together with the Navier Stokes equation and the continuous surface stress with no smoothing formulation incorporating surfactant with the code SURFER++. The computations were performed in the computational domain 2 x $\frac{1}{2}$ x 1, with a $\frac{1}{64}$ spatial mesh and an initial drop radius $a = 0.125$.

Time Step	Re_D	Ca_D	$radius_D$	$Volume_D$	Time to Break
(s)			(x10^{-2})	(x10^{-3})	(seconds)
$10^{-3}\dot{\gamma}^{-1}$	6.2208	0.1104	9.859	4.01	24
$10^{-4}\dot{\gamma}^{-1}$	6.2264	0.1104	9.863	4.01	24
—% Error—	0.09	0	0.04	0	0

Table 6.2: Refined Time Step: Error Measurment for Re=10, Ca=0.14, Ca_e=0.155, r=0.1, Breakup sequence

Refining time step results in practically identical simulations. Visually, there is no difference in the output. Numerical error is within acceptable limits so the less refined time step is appropriate.

See Figure 6.2.

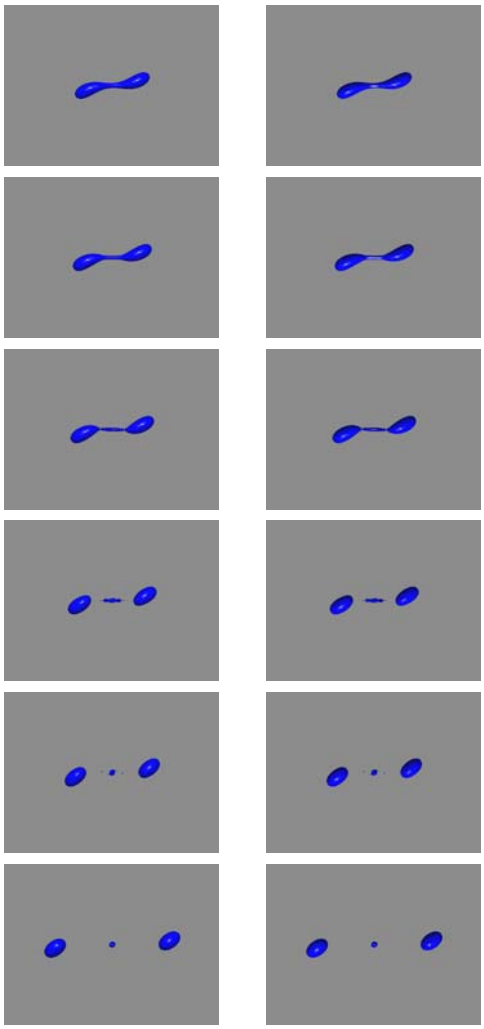

Figure 6.2: Refined Time Step: Visual Breakup Sequence for Re=10, Ca=0.14, Ca_e=0.155, r=0.1, Left: Timestep=$10^{-3}\dot{\gamma}^{-1}$, Right: Timestep=$10^{-4}\dot{\gamma}^{-1}$, Top to Bottom: Time = 21, 22, 23, 24, 25, 30 seconds

6.3 Changing box size

An expanded computational box size of 3 x $\frac{1}{2}$ x 1 was evaluated and compared to a similar run using a computational box size of 2 x $\frac{1}{2}$ x 1. We extend only the x-direction as this represents the direction of largest motion.

Table 6.3 compares the data generated for a typical breakup sequence. The data are the result of a full simulation of the initial value problem, together with the Navier Stokes equation and the continuous surface stress with no smoothing formulation incorporating surfactant with the code SURFER++. The computations were performed with a $\frac{1}{64}$ spatial mesh, an initial drop radius $a = 0.125$, and timesteps = $10^{-3}\dot{\gamma}^{-1}$.

Computational Box Size (s)	Re_D	Ca_D	$radius_D$ (x10^{-2})	$Volume_D$ (x10^{-3})	Time to Break (seconds)
2 x $\frac{1}{2}$ x 1	6.2208	0.1104	9.859	4.01	24
3 x $\frac{1}{2}$ x 1	6.2207	0.1104	9.859	4.01	24
—% Error—	0.0016	0	0	0	0

Table 6.3: Expanded Computational Box: Error Measurment for Re=10, Ca=0.14, Ca_e=0.155, r=0.1, Breakup sequence

Numerical data for both simulations is very comparable. There are slight visual differences in the neck region at break, but this is superficial. A 2 x $\frac{1}{2}$ x 1 computation box size is acceptable. See Figure 6.3.

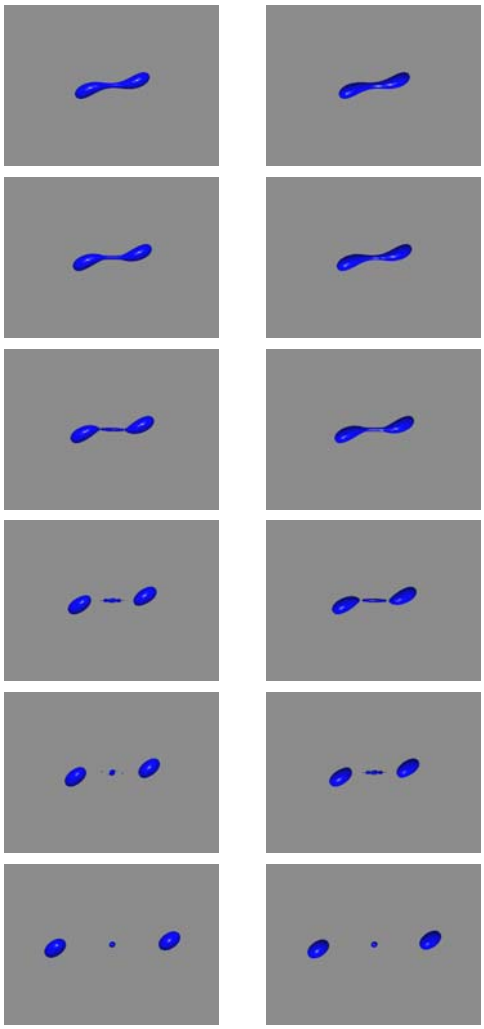

Figure 6.3: Expanded Computational Box: Visual Breakup Sequence for Re=10, Ca=0.14, Ca_e=0.155, r=0.1, Left: Box = 2 x $\frac{1}{2}$ x 1, Right: Box = 3 x $\frac{1}{2}$ x 1, Top to Bottom: Time = 21, 22, 23, 24, 25, 30 seconds

Bibliography

[1] Jie Li, Yuriko Y. Renardy, and Michael Renardy, *Numerical simulation of breakup of a viscous drop in simple shear flow through a volume-of-fluid method,* Physics of Fluids, **12**(2), 269–282 (2000).

[2] Denis Gueyffier, Jie Li, Ali Nadim, Ruben Scardovelli, and Stéphane Zaleski, *Volume-of-Fluid Interface Tracking with Smoothed Surface Stress Methods for Three-Dimensional Flows,* Journal of Computational Physics, **152**, 426–456 (1999).

[3] H. A. Stone, *A simple derivation of the time-dependent convective-diffusion equation for surfactant transport along a deforming interface,* Physics of Fluids A, **2**(1), 111–112 (1990).

[4] S. S. Sadhal, *Stokes flow past bubbles and drops partially coated with thin films. Part 1. Stagnant cap of surfactant film - exact solution,* Journal of Fluid Mechanics, **126**, 237–250 (1983).

[5] M. Tjahjadi, H. A. Stone, and J. M. Ottino, *Satellite and subsatellite formation in capillary breakup,* Journal of Fluid Mechanics, **243**, 297–317 (1992).

[6] H. A. Stone and L. G. Leal, *The effects of surfactants on drop deformation and breakup,* Journal of Fluid Mechanics, **220**, 161–186 (1990).

[7] R. E. Davis and Andreas Acrivos *The influence of surfactants on the creeping motion of bubbles,* Chemical Engineering Science, **21**, 681–685 (1966).

[8] H. A. Stone and L. G. Leal, *The influence of initial deformation on drop breakup in subcritical time-dependent flows at low Reynolds numbers,* Journal of Fluid Mechanics, **206**, 223–263 (1989).

[9] Charles Eggleton, Yashodhara P. Pawar, and Kathleen J. Stebe, *Insoluble surfactants on a drop in an extensional flow: a generalization of the stagnated surface limit to deforming interfaces,* Journal of Fluid Mechanics, **385**, 79–99 (1999).

[10] Ruben Scardovelli and Stéphane Zaleski, *Direct Numerical Simulation of Free-Surface and Interfacial Flow,* Annu. Rev. Fluid Mechanics, **31**, 567–603 (1999).

[11] Z. He, C. Maldarelli, and Z. Dagan, *The Size of Stagnant Caps of Bulk Soluble Surfactant on the Interfaces of Translating Fluid Droplets,* Journal of Colloid and Interface Science, **146**(2), 442–451 (1991).

[12] Y. Renardy, V. Cristini, and J. Li, *Drop fragment distributions under shear with inertia,* International Journal of Multiphase Flow, To appear.

[13] Adrian V. Coward, Yuriko Y. Renardy, Michael Renardy, and John R. Richards, *Temporal Evolution of Periodic Disturbances in Two-Layer Couette Flow,* Journal of Computational Physics, **132**, 346–361 (1997).

[14] Jie Li, Yuriko Y. Renardy, and Michael Renardy, *A numerical study of periodic disturbances on two-layer Couette flow,* Physics of Fluids, **10**(12), 3056–3071 (1998).

[15] Yuriko Y. Renardy, Michael Renardy, and Vittorio Cristini, *A new volume-of-fluid formulation for surfactants and simulations of drop deformations under shear at a low viscosity ratio,* European Journal of Mechanics B/Fluids, **21**, 49–59 (2001).

[16] Rutherford Aris, *Vectors, Tensors, and the Basic Equations of Fluid Mechanics,* Dover Publications, Inc., New York, 1962.

[17] G. K. Batchelor, *An Introduction to Fluid Dynamics,* Cambridge University Press, United Kingdom, 1967.

[18] Chia-Shun Yih, *Fluid Mechanics, A Concise Introduction to the Theory,* McGraw-Hill Book Company, New York, 1969.

[19] Daniel D. Joseph and Yuriko Y. Renardy, *Fundamentals of Two-Fluid Dynamics, Part 1: Mathematical Theory and Applications,* Springer-Verlag, New York, 1991.

[20] Robert A. Granger, *Fluid Mechanics,* Dover Publications, Inc., New York, 1985.

[21] H. P. Grace, *Dispersion phenomena in high viscosity immiscible fluid systems and application of static mixers as dispersion devices in such systems,* Chem. Eng. Commun., **14**, 225 (1982).

[22] Yuriko Y. Renardy, Vittorio Cristini, *Effect of inertia on drop breakup under shear,* Physics of Fluids, **13**(1), 7–13, (2001).

[23] J. M. Rallison, *The deformation of small viscous drops and bubbles in shear flows,* Annu. Rev. Fluid Mech., **16**, 45 (1984).

[24] H. A. Stone, *Dynamics of drop deformation and breakup in viscous fluids,* Annu. Rev. Fluid Mech., **26**, 65 (1994).

[25] S. Kwak and C. Pozrikidis, *Adaptive triangulation of evolving closed, or open surfaces by the advancing front method,* J. Comput. Phys., **14**, 61 (1998).

[26] V. Cristini, J. Blaqzdziewicz, and M. Loewenberg, *Drop breakup in three-dimensional viscous flows,* Phys. Fluids, **10**, 1781 (1998).

[27] S. Guido and M. Villone, *Three-dimensional shape of a drop under simple shear flow,* J. Rheol., **42**, 395 (1998).

[28] J. U. Brackbill, D. B. Kothe, and C. Zemach, *A continuum method for modeling surface tension,* J. Comput. Phys., **100**, 335 (1992).

[29] B. Lafaurie, C. Nardone, R. Scardovelli, S. Zaleski, and G. Zanetti, *Modelling merging and fragmentation in multiphase flows with SURFER,* J. Comput. Phys., **113**, 134 (1994).

[30] J. Li, *Calcul d'Interface Affine par Morceaux (Piecewise Linear Interface Calculation),* C.R.Acad.Sci., Ser. IIb: Mec., Phys., Chim., Astron., **320**, 391 (1995).

[31] J. Li, *Résolution numérique de l'équation de Navier-Stokes avec reconnexion d'interfaces. Méthode de suivi de volume et application à l'atomisation (Numerical resolution of the Navier-Stokes equation with reconnection of interfaces. Volume of fluid method with applications)*, Thése de Doctorate de Universitè Pierre et Marie Curie (Paris VI) (1996).

[32] R. Scardovelli and S. Zaleski, *Direct numerical simulation of free surface and interfacial flow,* Annu. Rev. Fluid Mech., **31**, 567 (1999).

[33] T. Y, Hou, J. S. Lowengrub, and M. J. Shelley, *The long-time motion of vortex sheets with surface tension,* Phys. Fluids, **9**, 1933 (1997).

[34] J. Li and Y. Renardy, *Direct simulation of unsteady axisymmetric core-annular flow with high viscosity ratio,* J. Fluid Mech., **391**, 123 (1999).

[35] A.J. Chorin, *A numerical method for solving incompressible viscous flow problems,* J. Comput. Phys., **2**, 12 (1967).

[36] W. J. Rider and D. B. Kothe, *Reconstructing volume tracking,* J. Comp Phys., **141**, 112 (1998).

[37] D. B. Kothe, M. W. Williams and E. G. Puckett, *Accuracy and convergence of continuum surface tension models,* in Fluid Dynamics at Interfaces (W. Shyy and R. Narayanan, ed.), Cambridge University Press, 1998, pp 294-305.

[38] G. I. Taylor, *The viscosity of a fluid containing small drops of another fluid,* Proc. R. Soc. London, Ser. A., **138**, 41 (1932).

[39] G. I. Taylor, *The formation of emulsions in definable fields of flow,* Proc. R. Soc. London, Ser. A, **146**, 501 (1934).

[40] Y. Renardy and J. Li, *Parallelized simulations of two-fluid dynamics,* in Applications on Advanced Architecture Computers (Greg Astfalk, ed.), SIAM News, Dec 2000, pp 1-15.

[41] S. Popinet and S. Zaleski, *A front-tracking algorithm for the accurate representation of surface tension,* Int. J. Numer. Methods Fluids, **30**, 775 (1999).

[42] C. R. Marks, *Drop breakup and deformation in sudden onset strong flows,* Ph.D. Thesis, University of Maryland at College Park (1998).

[43] Y. Pawar and K. J. Stebe, *Marangoni effects on drop deformation in an extensional flow: The role of surfactant physical chemistry. I. Insoluble surfactants,* Phys. Fluids, **8**(7), 1738 (1996).

[44] C. .D. Eggleton, T. Tsai and K. J. Stebe, *Tip streaming from a drop in the presence of surfactants,* Phys. Rev. Lett., **87**(4), Article 048302-1 (2001).

[45] C. D. Eggleton and K. J. Stebe, *An adsorption-desorption-controlled surfactant on a deforming droplet,* J. Colloid Interf. Sci., **208**, 68 (1998).

[46] J. K. Ferri, S. Y. Lin and K. J. Stebe, *Curvature effects in the analysis of pendant bubble data: comparison of numerical solutions, asymptotic arguments, and data,* J. Colloid Interf. Sci., **241**, 154 (2001).

[47] M. Mulqueen, S. S. Datwani, K. J. Stebe and D. Blankschtein, *Dynamic surface tension of aqueous surfactant mixtures: experimental investigation,* Langmuir, **17**, 7494 (2001).

[48] Steve Yon and C. Pozrikidis, *A finite-volume/boundary-element method for flow past interfaces in the presence of surfactants, with application to shear flow past a viscous drop,* Computers and Fluids, **27**(8), 879 (1998).

[49] Yuriko Y. Renardy and Vittorio Cristini, *Scalings for fragments produced from drop breakup in shear flow with inertia,* Phys. Fluids, **13**(8), 2161 (2001).

[50] Xiaofan Li and C. Pozrikidis, *The effects of surfactants on drop deformation and on the rheology of dilute emulsions in Stokes flow,* J. Fluid Mech., **341**, 165 (1997).

[51] C. Pozrikidis, *Numerical studies of cusp formation at fluid interfaces in Stokes flow,* J. Fluid Mech., **357**, 29 (1998).

[52] W. J. Milliken, H. A. Stone and L. G. Leal, *The effect of surfactant on the transient motion of Newtonian drops,* Phys. Fluids A, **5**(1), 69 (1993).

[53] R. A. De Bruijn, *Tipstreaming of drops in simple shear flows,* Chemical Engineering Science, **48**(2), 277, (1993).

Vita

Mary Ann Drumright-Clarke

Education

Ph.D., Mathematics, 2002, Virginia Polytechnic Institute and State University
M.S., Mathematics, 1999, Virginia Polytechnic Institute and State University
B.S., Materials Engineering, 1991, Virginia Polytechnic Institute and State University

Work Experience

Research Engineer, Southwest Research Institute, San Antonio, TX, June 2002
Graduate Teaching and Research Assistant, Virginia Polytechnic Institute and State University, Blacksburg, VA, 1996 - 2002
Process Development Engineer, Siecor Corporation, Hickory, NC, 1993 - 1996
Materials Engineer, Siecor Corporation, Hickory, NC, 1991 - 1993
Engineering Technician, AT&T Microelectronics, Richmond, VA, 1988 - 1991

Publications

Y. Renardy, S. Popinet, L. Duchemin, M. Renardy, M.A. Clarke, S. Zaleski, C. Josserand, 2001, *Numerical simulation of a water drop impacting a superhydrophobic surface*, Under revision.
B. Khomami, Y. Renardy, K.C. Su, M.A. Clarke, 2000, *An experimental/theoretical investigation of interfacial stability in superposed pressure-driven channel flow of Newtonian and well-characterized viscoelastic fluids. Part II: Nonlinear stability*, J. Non-Newtonian Fluid Mech. 91/1, pp.85-104.
US Patent 6171526. Jan 9, 2001. W. McAlpine, M.A. Clarke, *Method for making a grooved spacer for telecommunications cable.*
US Patent 6066798. May 23, 2000. W. McAlpine, M.A. Clarke, *Slotted core telecommunications cable.*
US Patent 5830517. Nov 3, 1998. M.A. Clarke, C. Eoll, *Method and apparatus for use in the manufacture of optical cable slotted rods.*
US Patent 5830516. Nov 3, 1998. W. McAlpine, M.A. Clarke, *Apparatus and method for making a grooved spacer for telecommunications cable.*
US Patent 5388175. Feb 7, 1995. M.A. Clarke, *Optical cable having powder embedded in plastic surfaces.*

Personal History

Born: September 22, 1969, Emporia, KS, USA
Parents: Arthur Lee Drumright and Patricia Ann DuBois-Drumright, Richmond, VA, USA
Siblings: Ray Eugene Drumright, Midland, MI and Laura Lynn Drumright-Hill, Wilmington, DE
Spouse: Michael Gordon Clarke

Mary Ann Drumright-Clarke is the product of both Canadian and American public school systems. Her early childhood was spent in various cities and towns including Emporia, Kansas; Richmond, Virginia; Collingwood, Ontario; Frederick, Oklahoma; Richardson, Texas; and then Richmond, Virginia again. She attended three different high schools, but matriculated from Meadowbrook High School in Chesterfield County, Virginia in 1986. Immediately following high school, she attended Virginia Polytechnic Institute and State University in Blacksburg, Virginia. While there she participated in the cooperative education program and graduated with a degree in Materials Engineering. During her cooperative educational experience she met Michael Clarke, who became her husband soon after her graduation. She accepted engineering work in Hickory, North Carolina at the research, development and engineering center of Siecor Corporation, a fiber optic cabling subsidiary of Siemens, A.G. and Corning, Incorporated. While there she worked in materials selection and qualification and later in process development, primarily in extrusion and cabling. She returned to Virginia Polytechnic Institute and State University in the graduate field of mathematics to gain experience in process modeling through numerical programming and worked under the tutelage of Dr. Yuriko Renardy. After receiving her M.S. and Ph.D., she accepted employment as a research engineer in the engineering dynamics department of Southwest Research Institute in San Antonio, Texas.

Mary Ann is the proud aunt of seven nieces and nephews including (by age) Heather Wyatt, Amy Green, Ben Drumright, Aaron Green, Abby Drumright, Sarah Hill and Luke Drumright. She is the caretaker of two pets including Sheba, the love dog, and Patty, the killer cat.